Single-Site Approximations in the Electronic Theory of Simple Binary Alloys*

B. VELICKÝ,† S. KIRKPATRICK, AND H. EHRENREICH
Division of Engineering and Applied Physics, Harvard University, Cambridge, Massachusetts 02138
(Received 26 June 1968)

A single-band model Hamiltonian is used to describe the electronic structure of a three-dimensional disordered binary alloy. Several common theories based on the single-site approximation in a multiple-scattering description are compared with exact results for this Hamiltonian. The coherent-potential theory of Soven and others is shown to be the best of these. Within the appropriate limits, it exhibits dilute-alloy, virtual-crystal, and well separated impurity-band behavior. Hubbard and Onodera's and Toyozawa's simple model density of states is employed in numerical calculations for a wide variety of concentrations and scattering-potential strengths. Explicit results are exhibited for the total density of states, the partial density contributed by each component, and such k-dependent properties as the Bloch-wave spectral density and the distribution function. These illustrate the general conclusions as well as the limitations of the quasiparticle description.

I. INTRODUCTION

THIS paper is concerned with two aspects of the single-particle theory of the electronic structure of disordered binary alloys. It presents a systematic derivation of the so-called coherent-potential (CP) theory[1] of such systems, clarifies its meaning and limitations, and discusses numerical results for a moderately realistic single-band model corresponding to a three-dimensional system. In addition it presents a number of exact results for this model. These are useful as a basis for comparison with approximate calculations, and also when the two constituents give rise to two well-separated sub-bands, a situation in which the fluctuations of the random potential are so large that the CP theory is not expected to be valid.

The CP concept has generally been developed within the framework of the multiple scattering description[2] of disordered systems.[3–5] In this approach the propagation of an electron or lattice wave in an alloy is regarded as a succession of elementary scatterings on the random atomic scatterers, which are then averaged over all configurations of atoms. Taylor[6] and Soven,[1] dealing respectively with the case of the lattice vibration and electron-excitation spectrum in an alloy, returned to the Ewald-Lax theory[2] of multiple scattering. They viewed a given scatterer as being embedded in an effective medium whose choice was open and could be made self-consistently. This choice in turn determined an effective Hamiltonian called the coherent-potential Hamiltonian. The physical condition corresponding to this choice is simply that a single scatterer embedded in this effective medium should produce no further scattering on the average. The effective Hamiltonian in question is to be regarded as an unknown of the problem, and in contrast to the known "unperturbed" Hamiltonian that forms the usual starting points for multiple scattering theories, is not improved further by considering scattering corrections of ever increasing order. In this sense, the self-consistent choice of Hamiltonian is optimal among all single-site approximations, which neglect the scattering from clusters of atoms. Although the clustering effects may be important under certain circumstances, the single-site approximation renders the problem tractable. It may be said to play the same role in alloys as the molecular-field theory in magnetism.

McMillan and Anderson[7] used a similar approach[8] in their treatment of liquid iron. Crudely speaking, their model binary alloy consisted of iron atoms and vacancies. A quite different and important application of the same formalism was made very recently by Onodera and Toyozawa.[9] They described Frenkel excitons in mixed ionic crystals using a simple three-dimensional single-exciton band model which permits a detailed solution of the problem. In addition, quantities other than the density of states, namely the spectral density describing the optical absorption, were calculated and discussed for the first time. The CP approximation was there rightly regarded as a scheme which interpolates between properly described limits corresponding to the entire range of impurity concentrations and strong and weak scattering. A band model similar to that used by these authors, and previously introduced by Hubbard,[10] will also be employed here to ob-

* Supported in part by grant No. GP-8019 of the National Science Foundation and the Advanced Research Projects Agency.

† Permanent address: Institute of Solid State Physics, Czechoslovak Academy of Sciences, Prague.

[1] P. Soven, Phys. Rev. **156**, 809 (1967).

[2] M. Lax, Rev. Mod. Phys. **23**, 287 (1951).

[3] S. F. Edwards, Phil. Mag. **6**, 617 (1961).

[4] J. L. Beeby and S. F. Edwards, Proc. Roy. Soc. (London) **A274**, 395 (1963).

[5] A most useful recent source of references for the problem of liquid metals is the *Proceedings of the International Conference on the Properties of Liquid Metals, Brookhaven, 1966*, given in Advan. Phys. **16**, 147 (1967).

[6] D. W. Taylor, Phys. Rev. **156**, 1017 (1967).

[7] P. W. Anderson and W. L. McMillan, in *Proceedings of the International School of Physics "Enrico Fermi," Course 37*, edited by W. Marshall (Academic Press Inc., New York, 1967).

[8] For a different approach to dilute liquid alloys, see E. A. Stern, Phys. Rev. **168**, 730 (1968).

[9] Y. Onodera and Y. Toyozawa, J. Phys. Soc. Japan **24**, 341 (1968).

[10] J. Hubbard, Proc. Roy. Soc. (London) **A276**, 238 (1963).

tain the detailed results to be discussed in connection with Sec. IV.

The older attempts to obtain self-consistent description of mixed crystals dealt with phonons for low-impurity concentrations.[11,12] Also closely related were efforts by Hubbard to obtain a self-consistent description of electron correlations in narrow bands. In the third of a series of papers Hubbard[13] introduces an alloy analogy, and, by finding appropriate means of truncating coupled Green's-function equations, he arrives at a self-consistent formulation of the alloy problem, which we shall show in this paper to be precisely equivalent to the CP approximation. Indeed, the formalism and its physical interpretations in this more limited application to be presented here will be seen to be considerably simpler than that of Hubbard.

Since this paper will deal with a number of different aspects of the alloy problem, a fairly detailed outline of the various topics and principal conclusions, with reference to the sections where these are discussed, may be helpful. Section II provides a succinct and general derivation of all single-site approximations using multiple-scattering theory. This approach permits direct comparison of the coherent-potential approach with other single-site approximations since these approximations are all placed on the same footing. The principal assumption underlying this treatment is that the total scattering potential may be expressed as a sum of contributions due to single atomic scatterers. A single-site description of the alloy problem is seen to involve the following physical ingredients. The total scattered wave is composed of contributions from each atom, while the effective wave incident on a given atom excludes the contribution of that atom. This contribution is obtained as a product of the atomic t matrix and the effective wave. Both quantities are configuration dependent. The essence of the single-site approximation (SSA) is the assumption that these quantities are not statistically correlated. The atomic scattered wave therefore becomes upon averaging a product of the configurationally averaged t matrix and the averaged effective wave. This procedure therefore replaces the true medium surrounding a given site by an effective one.

Succeeding parts of the paper become increasingly specialized and the results obtained correspondingly more specific. In Sec. III a single-band model for the alloy Hamiltonian is introduced. In terms of the Wannier representation, each site is characterized by a single orbital. It is assumed that the "hopping integrals," describing the transfer of electrons between sites, are identical to those in either perfect crystal. Accordingly, only the diagonal elements of the alloy Hamiltonian are random. Significantly, the entire behavior of the Hamiltonian may be specified in terms of just two parameters characterizing the concentration and the strength of the random potential. The bandwidth, which is determined by the hopping integrals, simply scales the energies.

The discussion of Sec. III concerns only general properties which do not involve the SSA. Exact statements are made about the symmetries of the problem, the localization of the spectrum (Sec. III A), and the asymptotic behavior of various quantities of interest (Sec. III B). The latter results for the averaged Green's function and self-energy are important in particular because they yield information about the moments of the density of states, the spectral density for Bloch states, and, in addition, lead to a family of sum rules involving the self-energy (Sec. III B). Such information is useful in two respects: as a basis for judging the results of approximate treatments, and also as a source of valid statements in regimes such as that involving two well-separated sub-bands (the "split-band limit") where the strength of the random potential is sufficiently large that the SSA is likely to fail because of the prevailing large flucutations with respect to the effective medium[14] (Sec. III C). In the "split-band limit" the self-energy has a pole whose existence reflects the fact that the sub-bands are becoming nearly independent. This is a case of physical importance since the d bands arising from the two constituents in such alloys as brass (Cu and Zn) are well separated. Of course, the degeneracy of bands in this case prevents immediate application of the methods of this paper.

The final section (Sec. IV) of the paper is concerned with the single-site approximation as applied to the single-band model. The development previously given in Sec II is recapitulated for this particular case in Sec. IV A, and explicit expressions for the self-energy, the total density of states, and the density of states associated with each type of site obtained. This leads to a conservation condition relating the total charge density per site to that of each of the constituents, a condition which in Sec IV B is shown to be identical to the equation defining the CP approximation. After an examination of the appropriate perturbation limits corresponding to the dilute alloy,[15] virtual crystal,[16] and atomic limits,[10] the CP approximation is shown to be the best of all single-site descriptions (Sec. IV B). It interpolates properly between these various limits, leading to reasonable results for all alloy concentrations as well as a wide range of strengths of the random scattering potential. In addition, it will be shown to be better than the perturbation theoretic results in the limiting regimes.

[11] A. A. Maradudin, in *Brandeis Summer Institute 1962 Lectures* (W. A. Benjamin, Inc., New York, 1963), Vol. 2. For more recent references to work on lattice vibrations in disordered systems, see *Localized Excitations in Solids*, edited by R. F. Wallis (Plenum Press, Inc., New York, 1968).

[12] A. A. Maradudin, E. W. Montroll, and G. H. Weiss, in *Solid State Physics*, edited by F. Seitz and D. Turnbull (Academic Press Inc., New York, 1963), Suppl. 3.

[13] J. Hubbard, Proc. Roy. Soc. (London) **A281**, 401 (1964).

[14] I. M. Liftshiz, Usp. Fiz. Nauk **83**, 617 (1964) [English transl.: Soviet Phys.—Usp. **7**, 549 (1965)].

[15] G. F. Koster and J. C. Slater, Phys. Rev. **96**, 1208 (1954).

[16] L. Nordheim, Ann. Physik **9**, 607 (1931).

The considerations are made even more specific in Sec. IV C, where a particular form of the single-band density of states is introduced, which is sufficiently simple as to permit detailed numerical calculations of some single-particle quantities that are discussed in the last two subsections. In addition, some further CP results, not previously given, are introduced as they are needed for the discussion. Section IV D deals with the purely energy-dependent properties of the alloy, as described in the CP approximation, namely the self-energy, the density of states, and the local-state densities associated with each kind of site. Section IV E discusses the k dependent properties. The averaged Green's function in the Bloch representation is used to obtain specific results for the spectral density as well as the electron-distribution function in k space. The discussion of Secs. IV D and IV E is illuminated by fairly elaborate graphical displays which exhibit the variation of the quantities of physical interest for a wide range of parameters.

II. MULTIPLE-SCATTERING THEORY AND SINGLE-SITE APPROXIMATIONS

This section develops the formalism underlying the single-site approximation and derives results that are valid for any single-particle Hamiltonian which can be decomposed into a sum of contributions associated with each site.

We begin with the crystallographic description of the simple binary alloy to be considered: A strictly periodic lattice containing N equivalent sites is occupied by atoms of two kinds, A and B, in a random way. The respective concentrations per unit cell are x and $y=1-x$, both varying from 0 to 1. These conditions define a whole ensemble of possible arrays of atoms. We are interested only in the physical characteristics of the alloy averaged over this ensemble. The average of a quantity A will be denoted $\langle A\rangle$.

The electrons are described in the single-particle approximation. The one-electron Hamiltonian corresponding to a given configuration is denoted by H. This paper concerns only the single-particle properties, which are derived from the one particle Green's function

$$G(z)=(z-H)^{-1}. \tag{2.1}$$

In particular, $\langle G(z)\rangle$ determines all macroscopic quantities of interest. In contrast to G, the averaged $\langle G\rangle$ has the full symmetry of the empty lattice. The effective Hamiltonian characterizing the average crystal is defined by the equation

$$\langle G(z)\rangle=(z-H_{\text{eff}})^{-1}. \tag{2.2}$$

H_{eff} also has the full crystal symmetry, but is non-Hermitian and energy-dependent. It may be seen directly that H_{eff} is analytic in both complex half-planes and that

$$H_{\text{eff}}(z^*)=H^{\dagger}_{\text{eff}}(z). \tag{2.3}$$

If there is available some approximation $K=K(z)$ to the exact effective Hamiltonian which may be regarded as the starting approximation and which has the same analytic properties as H_{eff} the following identity may serve as an equation for $\langle G\rangle$:

$$\langle G\rangle=R+R(H_{\text{eff}}-K)\langle G\rangle. \tag{2.4}$$

Here,

$$R=(z-K)^{-1} \tag{2.5}$$

is the unperturbed Green's function.

In multiple-scattering theory an equivalent equation involving the T matrix replaces (2.4). The T matrix may be defined by the equation

$$G=R+RTR. \tag{2.6}$$

On averaging, the relation

$$\langle G\rangle=R+R\langle T\rangle R \tag{2.7}$$

between $\langle G\rangle$ and $\langle T\rangle$ is obtained. From (2.4) and (2.7), we obtain

$$H_{\text{eff}}=K+\langle T\rangle(1+R\langle T\rangle)^{-1}. \tag{2.8}$$

This equation can be used in two ways. Either the $\langle T[K]\rangle$ corresponding to a given K can be inserted in Eq. (2.8), or the equation

$$\langle T[K]\rangle=0 \tag{2.9}$$

may be used to determine K. Equation (2.8) then guarantees that the solution of (2.9) so obtained is just $K=H_{\text{eff}}$. These two possibilities define two different classes of approximate calculations of H_{eff}. The former, which may be termed non-self-consistent, is usually applicable only if there is available some small parameter like the concentration in a dilute alloy. As we shall see in Sec. IV B, this approach may lead to difficulties concerned with properly keeping terms to a given order in the small parameter used. By contrast, the latter self-consistent point of view resolves these difficulties and furthermore gives rise to an interpolation scheme which is valid over wide ranges of the parameters, like the concentration, characterizing the system. This approach, however, is less simple from the mathematical point of view.

The multiple-scattering method is applicable if we can decompose the random-perturbing potential $H-K$ into a sum of contributions of single scatterers associated with each site a_n, i.e.,

$$H-K=\sum_n V_n. \tag{2.10}$$

This condition is sufficiently general to be applicable to several cases of interest, such as the muffin-tin approximation and the single-band model to be described in the next section. V_n is not necessarily related directly to an atomic potential.

Combination of (2.6) and the identity

$$G=R+R(H-K)G \tag{2.11}$$

yields

$$T=(H-K)(1+RT). \tag{2.12}$$

Inserting (2.10) yields

$$T=\sum_n V_n(1+RT)\equiv\sum_n Q_n, \tag{2.13}$$

which expresses the T matrix as a sum of contributions arising from the individual scatterers. Introducing

$$T_n=(1-V_nR)^{-1}V_n, \tag{2.14}$$

the T matrix associated with site n, we obtain

$$Q_n=T_n(1+R\sum_{m\neq n}Q_m). \tag{2.15}$$

Equation (2.15) expresses the strength of a scatterer in the alloy as a product of the strength of an isolated scatterer and a factor describing the transformation of an unperturbed-wave incident on site n into an effective wave because of the multiple scattering in the alloy. The preceding equations represent a closed form of multiple-scattering theory. Inserting (2.15) into (2.13) and iterating we obtain the standard series[3]

$$T=\sum_n T_n+\sum_n T_nR\sum_{m\neq n}T_m+\cdots. \tag{2.16}$$

Relations (2.11)–(2.15) are exact. They lead to the exact averaged equations

$$\langle T\rangle=\sum_n\langle Q_n\rangle, \tag{2.17}$$

$$\langle Q_n\rangle=\langle T_n(1+R\sum_{m\neq n}Q_m)\rangle. \tag{2.18}$$

Equation (2.18) can be rewritten as

$$\langle Q_n\rangle=\langle T_n\rangle(1+R\sum_{m\neq n}\langle Q_m\rangle)+\langle T_nR\sum_{m\neq n}(Q_m-\langle Q_m\rangle)\rangle. \tag{2.19}$$

The first term in this equation describes the effect of the averaged effective wave seen by the nth atom, and the second term corresponds to fluctuations of the effective wave. Our basic approximation is to neglect this difficult term. We then obtain a closed set of equations,

$$\langle Q_n\rangle=\langle T_n\rangle(1+R\sum_{m\neq n}\langle Q_m\rangle), \tag{2.20}$$

for the averaged quantities. Using the fact that $\sum_{m\neq n}Q_m=T-Q_n$, we obtain

$$\langle Q_n\rangle=(1+\langle T_n\rangle R)^{-1}\langle T_n\rangle(1+R\langle T\rangle). \tag{2.21}$$

Substitution into (2.8) then yields the effective Hamiltonian

$$H_{\text{eff}}=K+\sum_n\langle T_n\rangle(1+R\langle T_n\rangle)^{-1}. \tag{2.22}$$

The quantity $\langle T_n\rangle(1+R\langle T_n\rangle)^{-1}$ is simply the effective scattering potential corresponding to the average scattering arising from the nth scatterer. Equation (2.22) replaces (2.8) in the single-site approximation and the discussion following (2.8) applies here as well without alterations. If some reasonable K is known, the single-scatterer T matrices can be obtained and (2.22) represents our final result. On the other hand, the self-consistency requirement (2.9) simplifies to

$$\langle T_n[K]\rangle=0 \tag{2.23}$$

for all n. Because of the periodicity of the averaged quantities, it is sufficient to consider only one, say the zeroth site. It should be mentioned that Eq. (2.23) is precisely identical with the conditions imposed by Soven[1] and Anderson and McMillan[7] to determine H_{eff}. The meaning of the single-site approximation may be understood by comparing Eqs. (2.15) and (2.20) which are seen to have identical structure. The decoupling of the two factors in Eq. (2.20) resulting from the neglect of the last term in (2.19) corresponds to the replacement of the factor describing the configuration dependent effective wave by a corresponding factor describing the surrounding alloy in an averaged way. The validity of the assumption that

$$\langle T_nR\sum_{m\neq n}(Q_m-\langle Q_m\rangle)\rangle=0 \tag{2.24}$$

depends on the neglect of all statistical correlations between n and all other sites m. These correlations are of two kinds resulting respectively from short range order and multiple scattering. The first of these has been eliminated by hypothesis. The other correlations, on the other hand, are always present. Their neglect is the fundamental assumption of a "molecular field" kind of theory involving only a single site surrounded by an averaged medium. In this connection it is to be emphasized that the character of the present approximation closely resembles that of the molecular-field theory of magnetism which also is valid for a wide range of parameters characterizing that particular problem. Of course the success of approximation (2.24) depends in practice on the choice of K. Of all choices the self-consistent solution $K=H_{\text{eff}}$ is to be preferred for several reasons which will be examined in detail later.

III. SINGLE-BAND MODEL: GENERAL PROPERTIES

This section discusses a single-band model which is closely related to the tight-binding approximation. Its main advantage is that it is quite tractable in the CP approximation. All matters relating to this approximation will be discussed in Sec. IV. The present section will develop the general properties of the model, which were already outlined in the Introduction.

A. Characterization of the Model

Although the model in question may be introduced purely formally, we prefer to motivate its definition physically. The ensuing discussion, however, will be less concerned with the physical realizability of the systems resulting when certain parameters are varied over wide ranges than with the general resulting behavior of various properties.

Consider an alloy described in the tight-binding approximation. A single atomic orbital $|n\rangle$ is associated with each site n. A single band would result in the case of a pure crystal. Accordingly, the term "single-band model" is used despite the fact that two sub-bands may occur in the alloy under certain conditions.

The one-electron Hamiltonian is

$$H=\sum_n |n\rangle\epsilon_n\langle n| +\sum_{n\neq m} |n\rangle t_{mn}\langle m| \tag{3.1}$$

$$\equiv D+W. \tag{3.2}$$

The second line defines the decomposition of H into a diagonal part D and an off-diagonal part W with respect to the Wannier representation. The matrix elements of H depend in general on the configuration of A and B atoms in the crystal.

The model is defined by the following assumptions, which are physically realizable when the orbitals are sufficiently localized and the atomic potentials are not too different.

(1) In the diagonal elements ϵ_n, the crystal field terms are assumed independent of the composition and the atomic configuration. Accordingly, these elements may be regarded as atomic levels which assume one of two possible values ϵ^A and ϵ^B depending on whether an atom A or B occupies n.

(2) The hopping integrals t_{nm} are assumed to be completely independent of alloy composition. The operator W may therefore be interpreted as the Hamiltonian of a pure crystal for which $\epsilon^A=\epsilon^B=0$. Similarly ϵ^A+W and ϵ^B+W, respectively, are the Hamiltonians for the pure A and B crystals.

In short, the elements of D are diagonal but random, whereas those of W are off-diagonal but translationally invariant.

The operator W is diagonal in the Bloch representation:

$$\langle k|W|k'\rangle=\delta_{kk'}\sum_n t_{0n}e^{i\mathbf{k}\cdot\mathbf{a}_n}\equiv\delta_{kk'}ws(k), \tag{3.3}$$

where

$$|k\rangle=N^{-1/2}\sum_n e^{i\mathbf{k}\cdot\mathbf{a}_n}|n\rangle \tag{3.4}$$

relates the Bloch and Wannier bases and w is one-half the bandwidth. The quantity $s(k)$, which describes the k dependence of the band energy, is dimensionless. In simple cases, such as nearest neighbor tight-binding bands in cubic lattices, $-1\leq s(k)\leq+1$. All that can be said for general bands, however, is that $\max s(k)\geq 0 \geq \min s(k)$ and

$$\max s(k)-\min s(k)=2. \tag{3.5}$$

It is also convenient to use the same energy units to express ϵ^A and ϵ^B, and to define the energy zero such that

$$\epsilon^A=\tfrac{1}{2}w\delta, \quad \epsilon^B=-\tfrac{1}{2}w\delta. \tag{3.6}$$

Equation (3.6) defines the dimensionless parameter

$$\delta=(\epsilon^A-\epsilon^B)/w. \tag{3.7}$$

For a given operator W the ensemble of Hamiltonians is completely specified in terms of two dimensionless parameters x and δ, respectively characterizing the concentration and the separation between atomic levels. The energy w simply scales the entire Hamiltonian. With some exceptions which will be explicitly indicated, we use energy units for which $w=1$.

Some convenient notation and formal relations will now be introduced.[17] Since $H_{\text{eff}}(z)$ has the full crystal symmetry, both it and $\langle G(z)\rangle=(z-H_{\text{eff}})^{-1}$ are diagonal in the k representation:

$$\langle k|H_{\text{eff}}(z)|k'\rangle=[s(k)+\Sigma(k,z)]\delta_{kk'}. \tag{3.8}$$

Equation (3.7) defines the quantity $\Sigma(k,z)$ which contains full information about the scattering corrections to the effective Hamiltonian. It is the self-energy with respect to the perfect crystal having Hamiltonian W. We also define

$$\mathcal{G}(k,z)\equiv\ll k|G(z)|k\gg=[z-s(k)-\Sigma(k,z)]^{-1}, \tag{3.9}$$

which is fully specified by the spectral density

$$\mathcal{A}(k,E)=-\pi^{-1}\,\mathrm{Im}\mathcal{G}(k,E+i0), \tag{3.10}$$

because the integral representation,

$$\mathcal{G}(k,z)=\int_{-\infty}^{\infty}\frac{dE}{z-E}\mathcal{A}(k,E), \tag{3.11}$$

is valid.

The (average) density of states per atom,

$$\rho(E)\equiv N^{-1}\,\mathrm{Tr}\langle\delta(E-H)\rangle, \tag{3.12}$$

may be expressed in terms of the Green's function as

$$\rho(E)=-(\pi N)^{-1}\,\mathrm{Im}\,\mathrm{Tr}\langle G(E+i0)\rangle. \tag{3.13}$$

The following explicit forms of (3.12), expressed respectively in the Wannier and Bloch representations, are also useful:

$$\rho(E)=-\pi^{-1}\,\mathrm{Im}\langle n=0|\langle G(E+i0)\rangle|n=0\rangle \tag{3.14}$$

$$=N^{-1}\sum_k \mathcal{A}(k,E). \tag{3.15}$$

Finally, we introduce the important auxiliary quantity[18]

$$F(z)\equiv N^{-1}\,\mathrm{Tr}\langle G(z)\rangle=\langle 0|\langle G(z)\rangle|0\rangle, \tag{3.16}$$

which, in view of (3.14), has the property

$$\rho(E)=-\pi^{-1}\,\mathrm{Im}F(E+i0), \tag{3.17}$$

so that

$$F(z)=\int_{-\infty}^{\infty}\frac{dE}{z-E}\rho(E). \tag{3.18}$$

As already mentioned, for given W, the alloy effective Hamiltonian is specified by x and δ. Here x ranges between 0 and 1, whereas δ can assume any (positive or negative) value. Any possible situation corresponds

[17] Our definitions are similar to those of Ref. 3.

[18] From now on, $|n=0\rangle$ will be denoted $|0\rangle$.

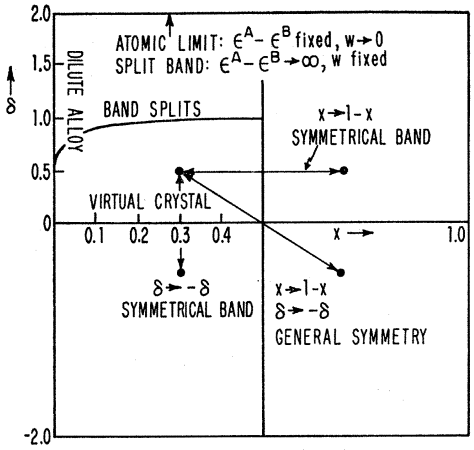

FIG. 1. Symmetries and limiting cases for the effective Hamiltonian as the parameters δ and x are varied. Arrows connect points equivalent under general and special symmetries. The line along which the band splits has been drawn for illustration only. For a specific case, see Fig. 4.

to a point in Fig. 1. The number of different cases that needs to be considered can be reduced by taking account of symmetry properties which $\mathcal{G}(k,z)$ satisfies. For purposes of the following discussion it is convenient to indicate the dependence on x and δ explicitly.

For any pure-crystal dispersion law $s(k)$

$$\mathcal{G}(k,z|x,\delta)=\mathcal{G}(k,z|1-x,-\delta), \tag{3.19}$$

$$\rho(E|x,\delta)=\rho(E|1-x,-\delta), \tag{3.20}$$

and similarly for $\Sigma(k,z)$. The point $(x,\delta)=(\frac{1}{2},0)$ in Fig. 1 is therefore a center of symmetry about which points in opposite quadrants are equivalent. Points in the neighboring quadrants can be related to each other when the pure-crystal band is symmetrical (like the nearest-neighbor tight-binding band in the bcc lattice). The additional symmetry obeyed by the density of states is[19]

$$\rho(E|x,\delta)=\rho(-E|1-x,\delta)=\rho(-E|x,-\delta). \tag{3.21}$$

The case of symmetrical bands is discussed more fully in Appendix A.

As a result of these symmetry arguments, only the quadrant $0\leq x\leq\frac{1}{2}$, $\delta\geq 0$ needs to be considered. The following physical limits can be identified:

(1) The line $x=0$ corresponds to the pure B crystal and its neighborhood to the dilute alloy case with A atoms playing the role of impurities.

(2) The line $\delta=0$ corresponds to the pure crystal described by the Hamiltonian W, Its vicinity is the virtual-crystal region, characterized by a single band which deviates but little from that of the pure crystal.

[19] Note that for the symmetrical band the density of states is an even function of E, which is consistent with (3.21) when $\delta=0$. This symmetry of ρ is preserved for $\delta\neq 0$ if $x=\frac{1}{2}$, again confirming (3.21).

(3) The case $\delta=(\epsilon_A-\epsilon_B)/w\to\infty$ may be obtained in two physically different ways. In the first, so-called atomic limit, the bandwidth $w\to 0$ and $\epsilon^A-\epsilon^B$ remains finite. On the other hand, w may be kept fixed and the level separation allowed to increase without limit. The latter case will be called the split-band limit. The atomic limit is simple because the spectrum consists of two atomic levels ϵ^A and ϵ^B. By contrast the split-band limit is never simple, for no matter how far the sub-bands are separated, there are always clusters of like atoms which produce molecular or bandlike splittings in the energy spectrum[14] which are of the order of w.[20]

The virtual crystal and split-band regimes may be defined more precisely in terms of δ with the help of a theorem concerning the localization of the spectrum.[21] For the present Hamiltonian H, it states the following: (1) For given W and δ and for any x the entire spectrum of H is contained in the union of the regions $(\epsilon^A+\min s(k), \epsilon^A+\max s)$ and $(\epsilon^B+\min s, \epsilon^B+\max s)$. (2) If the two regions do not intersect, there are just xN levels in the former and $(1-x)N$ in the latter.

Since $\max s-\min s=2$, the two intervals do not overlap for $|\delta|>2$. Accordingly $|\delta|\ll 2$ and $|\delta|\gg 2$ correspond respectively to the virtual crystal and split-band limits.

B. Moments

Practical methods for calculating the exact $\langle G\rangle$, even for the simple Hamiltonian under consideration here, are not readily available. It is, however, possible to study the exact asymptotic behavior of $\langle G\rangle$ as $z\to\infty$, and hence to obtain information about moments and sum rules of various quantities. The results and consequences of this kind of analysis will be explored in this and the following subsection, which are devoted respectively to general properties and those dealing with the split-band limit.

According to the localization theorem, the spectrum of the model Hamiltonian is bounded. Therefore $\langle G\rangle$ may be expanded in the form

$$\langle G\rangle=\langle(z-H)^{-1}\rangle=\sum_{p=0}^{\infty}\langle H^p\rangle/z^{p+1} \tag{3.22}$$

for sufficiently large z. A similar expansion of Eqs. (3.11) and (3.18) yields

$$\mathcal{G}(k,z)=\sum_{p=0}^{\infty}z^{-p-1}\int_{-\infty}^{\infty}dE\,E^p\mathcal{A}(k,E), \tag{3.23}$$

$$F(z)=\sum_{p=0}^{\infty}z^{-p-1}\int_{-\infty}^{\infty}dE\,E^p\rho(E). \tag{3.24}$$

[20] A. B. Harris and R. V. Lange [Phys. Rev. **157**, 295 (1967)] were the first to make a distinction between these limits, for the Hubbard Hamiltonian for interacting electrons in narrow bands.

[21] We have not found an adequate single reference for this well-known theorem. Useful discussions occur in Refs. 12 and 14, as well as on p. 712ff of A. Messiah, *Quantum Mechanics* (John Wiley & Sons, Inc., New York, 1962).

On the other hand, expansions of $\mathcal{G}(k,z)$ and $F(z)$ can be obtained by inserting (3.22) into their definitions (3.9) and (3.16). A comparison of the two expansions yields

$$M_p(k)\equiv\int dE\,E^p\mathcal{A}(k,E)=\langle k|\langle H^p\rangle|k\rangle, \quad (3.25)$$

$$\mu_p\equiv\int dE\,E^p\rho(E)=N^{-1}\,\mathrm{Tr}\langle H^p\rangle. \quad (3.26)$$

The preceding equations serve to define the moments M_p and μ_p of the spectral density and the density of states respectively. As a special case of (3.26), we define the moments $\mu_p{}^{(0)}$ of the pure crystal band ($\delta=0$) as

$$\mu_p{}^{(0)}\equiv\int dE\,E^p\rho^{(0)}(E)=N^{-1}\,\mathrm{Tr}W^p, \quad (3.27)$$

where $\rho^{(0)}$ is the appropriate density of states. Since W has no diagonal elements, $\mu_1{}^{(0)}=0$ in general. Furthermore, $\mu_{2p+1}{}^{(0)}=0$ for a symmetrical band since, in that case, $\rho^{(0)}(E)=\rho^{(0)}(-E)$.

The average $\langle H^p\rangle$ for small p and the resulting moments can be evaluated in straightforward fashion, as indicated in Appendix B. The results are given in Eqs. (3.29) and (3.30) in terms of the mean-atomic energy,

$$\epsilon=x\epsilon^A+y\epsilon^B, \quad (3.28)$$

and other previously defined quantities:

$$\begin{aligned}
&\langle H^0\rangle=1,\\
&\langle H^1\rangle=\epsilon+W,\\
&\langle H^2\rangle=\tfrac{1}{4}\delta^2+2\epsilon W+W^2,\\
&\langle H^3\rangle=\tfrac{1}{4}\epsilon\delta^2+(\tfrac{1}{2}\delta^2+\epsilon^2)W+3\epsilon W^2+W^3,\\
&\langle H^4\rangle=\tfrac{1}{16}\delta^4+xy\delta^2\mu_2{}^{(0)}+\epsilon\delta^2W+(\tfrac{3}{4}\delta^2+3\epsilon^2)W^2\\
&\qquad\qquad+4\epsilon W^3+W^4, \qquad (3.29)\\
&\langle H^5\rangle=\tfrac{1}{16}\epsilon\delta^4+xy\epsilon\delta^2\mu_2{}^{(0)}+xy\delta^2\mu_3{}^{(0)}\\
&\qquad+[(3/16)\delta^4+\tfrac{1}{2}\epsilon^2\delta^2+2xy\delta^2\mu_2{}^{(0)}]W\\
&\qquad+[\epsilon^3+(9/4)\epsilon\delta^2]W^2+(\delta^2+6\epsilon^2)W^3+5\epsilon W^4+W^5;\\
&\mu_0=1,\\
&\mu_1=\epsilon,\\
&\mu_2=\tfrac{1}{4}\delta^2+\mu_2{}^{(0)},\\
&\mu_3=\tfrac{1}{4}\epsilon\delta^2+3\epsilon\mu_2{}^{(0)}+\mu_3{}^{(0)}, \qquad (3.30)\\
&\mu_4=\tfrac{1}{16}\delta^4+(\delta^2+2\epsilon^2)\mu_2{}^{(0)}+4\epsilon\mu_3{}^{(0)}+\mu_4{}^{(0)},\\
&\mu_5=\tfrac{1}{16}\epsilon\delta^4+(5/2)\epsilon\delta^2\mu_2{}^{(0)}+[(5/4)\delta^2+5\epsilon^2]\mu_3{}^{(0)}\\
&\qquad\qquad+5\epsilon\mu_4{}^{(0)}+\mu_5{}^{(0)}.
\end{aligned}$$

$\langle H^p\rangle$ is seen to be a polynomial of degree p in W. The moments $M_p(k)$ of the spectral density have the same structure as the expressions in Eq. (3.29). They are obtained from (3.29) by replacing W^p by $s^p(k)$.

The asymptotic behavior of H_{eff} can be obtained from that of $\langle G\rangle$ given in (3.22). Solving Eq. (2.2), $\langle G\rangle=(z-H_{\mathrm{eff}})^{-1}$, for H_{eff} and substituting (3.22) yields

$$H_{\mathrm{eff}}=z[1-(1+\langle H\rangle z^{-1}+\langle H^2\rangle z^{-2}+\cdots)^{-1}], \quad (3.31)$$

so that, in view of (3.29),

$$H_{\mathrm{eff}}=\epsilon+W+\textstyle\sum_{p=1}^{\infty}\Lambda_p z^{-p}. \quad (3.32)$$

The operators Λ_p are determined most simply by substituting (3.22) and (3.32) into (2.2) and comparing equal powers of z^{-1}. The final result is

$$\begin{aligned}
H_{\mathrm{eff}}(z)=\epsilon+W+xy\delta^2[&z^{-1}-\epsilon z^{-2}+(\epsilon^2+\mu_2{}^{(0)})z^{-3}\\
&+(\mu_3{}^{(0)}-\epsilon^3-\epsilon\mu_2{}^{(0)})z^{-4}]+\cdots. \quad (3.33)
\end{aligned}$$

Surprisingly, the operators Λ_p turn out to be numbers at least to order z^{-4}. Using (3.8), we find

$$\begin{aligned}
\Sigma(k,z)=\epsilon+xy\delta^2[&z^{-1}-\epsilon z^{-2}+(\epsilon^2+\mu_2{}^{(0)})z^{-3}\\
&+(\mu_3{}^{(0)}-\epsilon^3-\epsilon\mu_2{}^{(0)})z^{-4}]+\cdots. \quad (3.34)
\end{aligned}$$

It is seen that $\Sigma(k,z)$ is independent of k to the same order. Because of the analyticity of H_{eff} in both half planes, Eq. (2.3), and the asymptotic form (3.34), the following dispersion relation for $\Sigma(k,z)$ can be derived:

$$\Sigma(k,z)=\epsilon+\pi^{-1}\int_{-\infty}^{\infty}\frac{dE}{E-z}\,\mathrm{Im}\Sigma(k,E+i0). \quad (3.35)$$

Expanding the right-hand side and comparing with (3.34) yields a family of sum rules of which the lowest are

$$\int_{-\infty}^{\infty}dE\,\mathrm{Im}\Sigma(k,E+i0)=-\pi xy\delta^2, \quad (3.36)$$

$$\int_{-\infty}^{\infty}dE\,E\,\mathrm{Im}\Sigma(k,E+i0)=\pi xy\epsilon\delta^2. \quad (3.37)$$

As will be seen in the next subsection, these relations provide useful physical insight concerning the lifetime of states $|k\rangle$ in the alloy.

C. Split-Band Limit

As an application of the results obtained so far, several properties of the system in the split-band limit will be derived. The localization theorem together with Eq. (3.5) imply that in this case the entire spectrum is confined to two well-separated regions, one centered around ϵ^A and the other around ϵ^B. The two portions of the spectrum will be termed "sub-bands" even though they may not consist of a simple continuum of levels. The sub-bands centered around ϵ^A and ϵ^B will be denoted, respectively, by α and β. For $\delta\to\infty$ sub-band α is associated entirely with A atoms and similarly for β with B. This correspondence is only approximate for δ large but finite.

Our first task will be to obtain some information concerning the moments

$$\mu_p{}^{\alpha,\beta}=\int_{-\infty}^{\infty}dE(E-\epsilon^{A,B})^p\rho^{\alpha,\beta}(E) \quad (3.38)$$

of the sub-band densities of states ρ^α and ρ^β which satisfy

$$\rho(E)=\rho^\alpha(E)+\rho^\beta(E). \tag{3.39}$$

The origins of energy here are shifted to the positions that are natural in the limit of well separated sub-bands.

The moments μ_p are easily expressed in terms of the $\mu_p{}^\alpha$, $\mu_p{}^\beta$. Using Eqs. (3.26) and (3.39), we write

$$\begin{aligned}\mu_p=&\int_{-\infty}^{\infty} dE(E-\epsilon^A+\epsilon^A)^p\rho^\alpha(E)\\ &+\int_{-\infty}^{\infty} dE(E-\epsilon^B+\epsilon^B)^p\rho^\beta(E)\\ =&\sum_{l=0}^{p}\binom{p}{l}[(\epsilon^A)^l\mu_{p-l}{}^\alpha+(\epsilon^B)^l\mu^\beta{}_{p-l}].\end{aligned} \tag{3.40}$$

This infinite set of equations can be solved in practice only by truncation. However, if the lowest n equations are considered by themselves, there are twice as many $\mu_p{}^{\alpha,\beta}$ as μ_p. This difficulty is not present in the split-band limit, since for large δ only the highest powers of ϵ^A, $\epsilon^B\sim\delta$ are important. The simplest example of this truncation procedure corresponds to $n=2$. The first two equations of (3.40) are

$$\mu_0=\mu_0{}^\alpha+\mu_0{}^\beta=1, \tag{3.41a}$$

$$\mu_1=\epsilon^A\mu_0{}^\alpha+\epsilon^B\mu_0{}^\beta+\mu_1{}^\alpha+\mu_1{}^\beta=\epsilon. \tag{3.41b}$$

Since all moments $\mu_p{}^{\alpha,\beta}$ are of order unity, the terms $\mu_1{}^\alpha$ and $\mu_1{}^\beta$ in (3.41b) are one order higher in δ^{-1} than the other terms and may be neglected. The resulting system of two equations now involves only two unknowns and may be solved to yield

$$\mu_0{}^\alpha=x+O(\delta^{-1}),\quad \mu_0{}^\beta=y+O(\delta^{-1}). \tag{3.42}$$

These results could have been predicted from the localization theorem since the moments $\mu_0{}^\alpha$ and $\mu_0{}^\beta$ simply correspond to the weights of the sub-bands.

By systematically neglecting terms of order δ^{-3} and higher, the six equations expressing $\mu_0\cdots\mu_5$ in terms of $\mu_0{}^{\alpha,\beta}\cdots\mu_2{}^{\alpha,\beta}$ may be solved in analogous fashion with the result

$$\begin{aligned}&\mu_0{}^\alpha=x+O(\delta^{-3}), && \mu_0{}^\beta=y+O(\delta^{-3}),\\ &\mu_1{}^\alpha=xy\mu_2{}^{(0)}/\delta+O(\delta^{-2}), && \mu_1{}^\beta=-xy\mu_2{}^{(0)}/\delta+O(\delta^{-2}),\\ &\mu_2{}^\alpha=x^2\mu_2{}^{(0)}+O(\delta^{-1}), && \mu_2{}^\beta=y^2\mu_2{}^{(0)}+O(\delta^{-1}).\end{aligned} \tag{3.43}$$

The first line of (3.43) again yields the result expected from the localization theorem. The second line involving $\mu_1{}^{\alpha,\beta}$ describes the mean shift from the atomic levels. This shift,

$$\mu_1{}^\alpha/\mu_0{}^\alpha=y\mu_2{}^{(0)}/\delta,\quad \mu_1{}^\beta/\mu_0{}^\beta=-x\mu_2{}^{(0)}/\delta, \tag{3.44}$$

increases the gap between α and β and is consistent with the repulsion of levels familiar from perturbation theory. For $x\to 0$, $\mu_1{}^\alpha/\mu_0{}^\beta$ approaches $\mu_2{}^{(0)}/\delta$, which is easily identified with the result for a single deep Koster-Slater impurity level.[15] The third line of (3.43), involving $\mu_2{}^{\alpha,\beta}$, is connected with the effective widths of the sub-bands. The widths are seen to approach finite values as $\delta\to\infty$.

More important for applications to actual solids is the variation of the width as a function of concentration x for fixed but large δ. Consider the α band and assume its variation with x can be described by a simple affine transformation:

$$\rho^\alpha(E-\epsilon^A|x)=\lambda_1\rho^\alpha[(E-\epsilon^A)/\lambda_2|x=1]. \tag{3.45}$$

We assume δ so large that the shifts (3.44) may be neglected. It is readily seen from (3.38) that $\mu_0{}^\alpha$ and $\mu_2{}^\alpha$ are obtained correctly only if

$$\lambda_1=\lambda_2=\sqrt{x}. \tag{3.46}$$

Even when the simple assumption (3.45) is not precisely valid one might still expect the effective height and width of the α sub-band to vary roughly as $\sqrt{x}$. The results for the β sub-band are analogous.

The sub-band moments of the spectral density,

$$M_p{}^{\alpha,\beta}(k)\equiv\int_{-\infty}^{\infty} dE(E-\epsilon^{A,B})^p\mathcal{A}^{\alpha,\beta}(k,E), \tag{3.47}$$

can be treated in the same manner as those of the density of states. The results for the α sub-band are

$$\begin{aligned}M_0{}^\alpha(k)=&x+2xys(k)/\delta-3xy(x-y)[s^2(k)-\mu_2{}^{(0)}]\\ &/\delta^2+O(\delta^{-3}),\\ M_1{}^\alpha(k)=&x^2s(k)+[3x^2y(s^2(k)-\mu_2{}^{(0)})+xy\mu_2{}^{(0)}]\\ &/\delta+O(\delta^{-2}),\\ M_2{}^\alpha(k)=&x^2y\mu_2{}^{(0)}+x^3s^2(k)+O(\delta^{-1}).\end{aligned} \tag{3.48}$$

The corresponding results for the β sub-bands can be obtained by the transformations $\delta\to-\delta$ and $x\leftrightarrow y$. The relationships $\mu_p{}^{\alpha,\beta}=N^{-1}\sum_k M_p{}^{\alpha,\beta}(k)$ are easily verified.

We first discuss the spectral density function in the limiting case when δ is so large that the dependence of (3.48) on it may be neglected. The first line states that an electron in state k spends a fraction x of its time on A sites. The second line indicates that the center of gravity of the spectral function $\mathcal{A}^\alpha(k,E)$ lies at

$$E=\epsilon^A+M_1{}^\alpha(k)/M_0{}^\alpha(k)=\epsilon^A+xs(k). \tag{3.49}$$

The effective linewidth with respect to (3.49) is given approximately by

$$\begin{aligned}&\{M_2{}^\alpha(k)/M_0{}^\alpha(k)-[M_1{}^\alpha(k)/M_0{}^\alpha(k)]^2\}^{1/2}\\ &\qquad=(xy\mu_2{}^{(0)})^{1/2}.\end{aligned} \tag{3.50}$$

The linewidth is seen to be independent of the state $|k\rangle$ and, generally speaking, has the same magnitude as the shift $xs(k)$. However, for $x\to 1$, $xs(k)\to s(k)$ but $(xyM_2{}^{(0)})^{1/2}\to 0$. In this case the sharp Bloch eigenstates of the A crystal are obtained. On the other hand, for $x\to 0$ both $xs(k)$ and $(xyM_2{}^{(0)})^{1/2}$ tend to zero and

a sharp isolated impurity line centered at ϵ^A results. Again, the results for the β sub-band are symmetrical.

The preceding results concerning the $M_p^{\alpha,\beta}$ have been developed primarily in order to show that $\Sigma(k,z)$ has a pole in the split-band limit. This is accomplished most directly by finding the zeroes of $\mathcal{G}(k,z)$. We begin by expressing $\mathcal{G}(k,z)$ in terms of the $M_p^{\alpha,\beta}$. Outside the sub-bands $\mathcal{G}(k,z)$ is analytic. Equation (3.11) can then be written

$$\mathcal{G}(k,z)=\int_{-\infty}^{\infty}\frac{dE}{(z-\epsilon^A)-(E-\epsilon^A)}\mathfrak{A}^{\alpha}(k,E)+\int_{-\infty}^{\infty}\frac{dE}{(z-\epsilon^B)-(E-\epsilon^B)}\mathfrak{A}^{\beta}(k,E)$$
$$=\sum_{p=0}^{\infty}[M_p^{\alpha}(k)/(z-\epsilon^A)^{p+1}+M_p^{\beta}(k)/(z-\epsilon^B)^{p+1}]. \quad (3.51)$$

The fact that $\mathfrak{A}=\mathfrak{A}^{\alpha}+\mathfrak{A}^{\beta}$ has been used. A few terms of the series (3.51) suffice for energies far removed from both sub-bands. However, when δ is large this applies even to the region between the sub-bands on the real axis. In this case, we have already seen in the results of Eq. (3.48) that the moments appearing in (3.51) are readily calculable. Accordingly, $\mathcal{G}(k,z)$ can be obtained to order δ^{-2} under these circumstances.

The zeroes of $\mathcal{G}(k,z)$ for finite z coincide with poles of $\Sigma(k,z)$ according to (3.9). Because there are just two sub-bands, there is at most one such point on the real axis located between the sub-bands. It is easily proved that provided $\delta\gg1$, $x\delta\gg1$, $y\delta\gg1$, the zero of $\mathcal{G}(k,z)$ exists and is located at $-\epsilon$, i.e.,

$$\mathcal{G}(k,-\epsilon)=0+O(\delta^{-3}). \quad (3.52)$$

Furthermore,

$$-(\partial/\partial z)\mathcal{G}(k,-\epsilon)=(xy\delta^2)^{-1}[1+\mu_2^{(0)}/xy\delta^2+O(\delta^{-3})]\approx(xy\delta^2-\mu_2^{(0)})^{-1}. \quad (3.53)$$

In the vicinity of $-\epsilon$,

$$\mathcal{G}(k,z)\approx-(xy\delta^2-\mu_2^{(0)})^{-1}(z+\epsilon). \quad (3.54)$$

Comparison with Eq. (3.9) shows that

$$\Sigma(k,z)=(xy\delta^2-\mu_2^{(0)})(z+\epsilon)^{-1}+\text{regular part}, \quad (3.55)$$

and that, accordingly, $\Sigma(k,z)$ has a pole at $-\epsilon$ for any k.

Such a pole will contribute significantly to the sum rules (3.36) and (3.37). However, its entire contribution falls into the region of zero spectral density, and therefore is not by itself physically significant. Instead, we wish to know the contribution of the individual sub-bands to the sum rules to order δ^{-2}. After subtraction of the contribution of the pole, the sum rules become

$$\int_{(\alpha)}dE\,\mathrm{Im}\Sigma(k,E+i0)+\int_{(\beta)}dE\,\mathrm{Im}\Sigma(k,E+i0)=-\pi\mu_2^{(0)}, \quad (3.56)$$

$$\epsilon^A\int_{(\alpha)}dE\,\mathrm{Im}\Sigma(k,E+i0)+\epsilon^B\int_{(\beta)}dE\,\mathrm{Im}\Sigma(k,E+i0)=\pi\epsilon\mu_2^{(0)}, \quad (3.57)$$

where the integration over the sub-bands is indicated symbolically by (α) and (β). The contribution of the individual sub-bands to (3.56),

$$\int_{(\alpha)}dE\,\mathrm{Im}\Sigma(k,E+i0)=-\pi y\mu_2^{(0)},\qquad \int_{(\beta)}dE\,\mathrm{Im}\Sigma(k,E+i0)=-\pi x\mu_2^{(0)}, \quad (3.58)$$

is obtained by solving the simultaneous equations. The results are seen to be independent of δ for large δ, which corresponds to the intuitive feeling that the sub-bands should become independent in this limit. Equation (3.58) show that the damping in the β sub-band and x decrease together, and similarly for the α sub-band. Although this behavior is expected to hold as $x\to0$, the derivation fails when x is too small. In this case $-\epsilon\to\epsilon^A$ and $\mathcal{G}(k,-\epsilon)$ can no longer be described using a few terms of (3.51).

IV. SINGLE-BAND MODEL: SINGLE-SITE APPROXIMATIONS

In this section the formalism of Sec. II is applied to the single-band model introduced in Sec. III. The first two subsections deal with general equations for the self-energy and compare several single-site approximations (SSA). Then a specific model density of states is introduced which is easily handled in computations. The last two subsections present numerical examples of some single-particle properties in the *CP* approximation for a wide range of concentrations and scattering potential strengths.

A. Basic Relations

In this subsection the general derivation of the effective-wave approximation given in Sec. II will be specialized to the single-band Hamiltonian discussed in Sec. III. At the outset it is necessary to make a reasonable and specific choice of the unperturbed Hamiltonian K which has so far not been explicitly defined. This choice must be both physically meaningful and tractable enough to be applicable to numerical calculations.

We define

$$K=W+\sum_n|n\rangle u(z)\langle n|=W+u(z)1, \quad (4.1)$$

where $u(z)$ and, hence, K is analytic everywhere except on the real axis and satisfies (2.3). It is seen from Eq. (4.1) that the term involving $u(z)$ is independent of k in Bloch representation, so that the entire k dependence is contained in W, or equivalently the function $s(k)$. This class of operators K is sufficiently broad to include the important dilute alloy, virtual crystal, and atomic limits. In addition, it includes the coherent potential, i.e., self-consistent single-site, effective Hamiltonian, which is of primary concern here.

In the ensuing discussion quantities related to the pure crystal having the Hamiltonian W for which $\delta=0$ will appear frequently. Although some of them have appeared previously [cf. (3.27)], we list them here for convenience:

$$G^{(0)}(z)=(z-W)^{-1},\quad \mathcal{G}^{(0)}(k,z)=[z-s(k)]^{-1},$$
$$\mathfrak{A}^{(0)}(k,E)=-\pi^{-1}\,\mathrm{Im}\mathcal{G}^{(0)}(k,E+i0)=\delta[E-s(k)], \quad (4.2)$$
$$\rho^{(0)}(E)=N^{-1}\sum_k \mathfrak{A}^{(0)}(k,E)=N^{-1}\sum_k \delta[E-s(k)],$$
$$F^{(0)}(z)=\int_{-\infty}^{\infty} dE(z-E)^{-1}\rho^{(0)}(E)$$
$$=N^{-1}\sum_k[z-s(k)]^{-1}.$$

For the K defined by (4.1), the unperturbed Green's function (2.5),

$$R(z)=(z-K)^{-1}$$
$$=[z-u(z)-W]^{-1}=G^{(0)}[z-u(z)], \quad (4.3)$$

can be expressed simply in terms of $G^{(0)}$. The function corresponding to (3.16) is then

$$\langle 0|R(z)|0\rangle=F^{(0)}(z-u(z))\equiv\hat{F}(z). \quad (4.4)$$

Matrix elements of K and related quantities are thus simply expressed in terms of the unperturbed quantities (4.2).

For H and K given by (3.1) and (4.1), respectively,

$$H-K=\sum_n|n\rangle[\epsilon_n-u(z)]\langle n|, \quad (4.5)$$

so that Eq. (2.10) is satisfied by the choice

$$V_n=|n\rangle[\epsilon_n-u(z)]\langle n|\equiv|n\rangle v_n\langle n|. \quad (4.6)$$

According to Eq. (2.14), and with the help of (4.4),

$$T_n(z)=|n\rangle v_n[1-v_n\hat{F}(z)]^{-1}\langle n|. \quad (4.7)$$

This expression is seen to be just the t matrix corresponding to a Slater-Koster impurity embedded at site n of a medium described by the Hamiltonian K.

The configurational average of (4.7) is

$$\langle T_n\rangle=|n\rangle\left[\frac{x[\epsilon^A-u]}{1-[\epsilon^A-u]\hat{F}}+\frac{y[\epsilon^B-u]}{1-[\epsilon^B-u]\hat{F}}\right]\langle n|$$
$$\equiv|n\rangle\{x\tau^A+y\tau^B\}\langle n|\equiv|n\rangle\tau\langle n|. \quad (4.8)$$

The approximate effective Hamiltonian (2.22) is then

$$H_{\mathrm{eff}}=W+\sum_n|n\rangle[u+\tau(1+\tau\hat{F})^{-1}]\langle n|. \quad (4.9)$$

Inserting (4.9) into (3.8) we obtain

$$\Sigma(k,z)\equiv\Sigma(z)=u(z)+\tau(z)[1+\tau(z)\hat{F}(z)]^{-1}, \quad (4.10)$$

where Σ is now k independent, a result which follows from (4.1) and the single-site approximation. The lack of k dependence may also be ascribed to this approximation.

The function $F(z)$ defined in Eq. (3.16) may now be simply expressed in terms of $F^{(0)}$ as defined in Eq. (4.2) by the same procedure as that used to arrive at Eq. (4.4),

$$F(z)=F^{(0)}[z-\Sigma(z)]. \quad (4.11)$$

The preceding expression leads immediately to the density of states $\rho(E)$ as defined by Eq. (3.17).

The SSA provides a means of studying the contribution of sites A and B to the total density of states. For the present simple model it is possible to give a precise, unambiguous definition of the average component density of states:

$$\rho^{A,B}(E)=-\pi^{-1}\,\mathrm{Im}\langle 0|\langle(E+i0-H^{A,B})^{-1}\rangle|0\rangle, \quad (4.12)$$

where $H^{A,B}$ is the Hamiltonian corresponding to a given alloy configuration with atoms A, B, respectively, located at the site $n=0$. These component densities are to be distinguished from the previously introduced $\rho^{\alpha,\beta}$ which referred to the density of states of the subbands α, β in the limiting split-band regime. When $\delta\to\infty$, $\rho^{\alpha,\beta}$ approaches $x\rho^A, y\rho^B$.

Since the entire ensemble of Hamiltonians H consists of two sub-ensembles composed of H^A and H^B, with weights x and y,

$$\rho(E)=x\rho^A(E)+y\rho^B(E), \quad (4.13)$$

as may be seen explicitly by comparing (3.17) and (4.12). This condition can be given a very simple physical interpretation. By integrating (4.13) over an arbitrary occupied portion of the band or sub-bands, the resulting condition $c=xc^A+yc^B$ states that the total charge density per atom is the sum of the densities due to A and B constituents properly weighted.

The effective wave approximation permits the explicit calculation of $\rho^{A,B}$ because the ensemble averaging in this case results in the replacement of ϵ_n by $\Sigma(z)$ everywhere except at the zeroth site where $\epsilon_0=\epsilon^{A,B}$. This is consistent with the single-site character of the approximation, i.e., that A, B are to be regarded as embedded in an effective crystal with Hamiltonian H_{eff}. Accordingly,

$$\langle 0|\langle(z-H^{A,B})^{-1}\rangle|0\rangle=\langle 0|[z-H_{\mathrm{eff}}(z)$$
$$-|0\rangle[\epsilon^{A,B}-\Sigma(z)]\langle 0|]^{-1}|0\rangle, \quad (4.14)$$

and, therefore,

$$\rho^{A,B}(E)=-\pi^{-1}\,\mathrm{Im}\{F[1-(\epsilon^{A,B}-\Sigma)F]^{-1}\}_{z=E+i0}. \quad (4.15)$$

As a result, Eq. (4.13) is seen to become the following condition for $\Sigma(z)$:

$$x[1-(\epsilon^A-\Sigma)F]^{-1}+y[1-(\epsilon^B-\Sigma)F]^{-1}=1, \quad (4.16)$$

where F itself depends on $\Sigma(z)$ because of Eq. (4.11).

B. Limiting Cases and CP Approximation

In this subsection we shall exhibit how nearly all common descriptions of alloys in various limiting cases, with the notable exception of effects connected with clustering, follow from the results in the SSA. In addition, we shall show that the CP approximation is simply the single-site approximation treated self-consistently. By explicit comparison of various aspects it will be seen that the CP approximation is the most satisfactory presently available for describing alloys for a wide range of parameters.

1. Dilute Alloy, $x \ll 1$

The unperturbed Hamiltonian K corresponds to the pure B crystal, i.e., $u(z)=\epsilon^B=-\frac{1}{2}\delta$. Only linear terms in x are retained in the expression (4.10). We obtain

$$\Sigma(z)=\epsilon^B+x\tau^A(z) \quad (4.17)$$

$$=\epsilon+x\delta^2F^{(0)}(z-\epsilon^B)[1-\delta F^{(0)}(z-\epsilon^B)]^{-1}, \quad (4.18)$$

where $\epsilon=\frac{1}{2}(x-y)\delta$ according to (3.28). Equation (4.17) describes the effect on the self-energy $\Sigma(z)$ of xN independent A impurities in the host B crystal.[22]

2. Virtual Crystal, $\delta \ll 1$

If results correct to first order in δ are sufficient, K may be taken to be W. In this case

$$\Sigma(z)=\epsilon, \quad (4.19)$$

which is simply the rigid-band approximation[23] corresponding to an undistorted shift of the band upon alloying. To order δ^2, $u(z)$ should be taken to be ϵ instead of zero. In this case we obtain

$$\Sigma(z)=\epsilon+xy\delta^2F^{(0)}(z-\epsilon), \quad (4.20)$$

a result familiar from the weak-coupling theory of Edwards.[3] The dependence on $xy\delta^2$ is to be particularly noted as a characteristic of such theories.[16]

3. Split Bands, $\delta \gg 1$

We recall that δ may be made large either by decreasing the bandwidth or increasing the separation of the atomic levels. A suitable K in the former case may by obtained, following Hubbard,[10] by setting

$$u(z)=\epsilon+xy\delta^2(z+\epsilon)^{-1}. \quad (4.21)$$

This choice is exact in the limit $\delta\to\infty$ when $W\to 0$ and hence $G=(z-D)^{-1}$. Using the scaling argument following Eq. (3.7), one might expect the preceding $u(z)$ to be valid in the split-band limit as well. However, it should be remembered from the discussion of Sec. III A that Eq. (4.21) neglects terms of order w which are unity in the split-band case and do not vanish as $\delta\to\infty$. Inserting (4.21) into (4.10) yields an expression for $\Sigma(z)$ which may be shown to be identical to that called the "scattering correction" by Hubbard.[13] Accordingly, Hubbard's truncation of his coupled Green's-function equations is equivalent to the SSA. Instead of discussing these results, however, we prefer, as Hubbard did, to deal more extensively with their self-consistent counterparts.

4. Coherent Potential Approximation: Self-Consistent Solution

So far we have used the first of the two approaches discussed after Eq. (2.8) to determine H_{eff}. Now we turn to the second approach of determining $K=H_{\text{eff}}$ on the basis of the self-consistency condition (2.9), which, in the effective wave approximation, reduces to (2.23), $T_n[K]=0$. For the present model T_n is given by (4.8) and therefore the self-consistency condition determining $u(z)=\Sigma(z)$, the only unknown part of K, is, according to (4.10),

$$\tau(z)=0. \quad (4.22)$$

Equation (4.22) may then be cast into the form

$$\Sigma(z)=\epsilon+xy\delta^2\frac{F^{(0)}[z-\Sigma(z)]}{1+[\Sigma(z)+\epsilon]F^{(0)}[z-\Sigma(z)]}, \quad (4.23)$$

which is identical to that given by Onodera and Toyozawa.[9] Alternatively, using (4.11), it can be cast into the form previously obtained by Soven,[1]

$$\Sigma(z)=\epsilon-[\epsilon^A-\Sigma(z)]F(z)[\epsilon^B-\Sigma(z)]. \quad (4.24)$$

Consequently, $\Sigma(z)$ is to be identified with Soven's Hamiltonian in the CP approximation. The equivalence of (4.24) to the self-consistent version of Hubbard's theory[13] is discussed in Appendix C. Equation (4.24), or its more convenient equivalent, (4.23), determines the CP Hamiltonian and is of central importance in the discussion to follow.

The rest of the subsection will be devoted to a comparison of the CP approximation with other single-site approximations. This discussion is intended to show that the CP approximation is preferable in many respects. For example, the simple physical condition of charge conservation (4.13) assumes the form (4.16) in the SSA. This is directly seen to be Eq. (4.24) slightly rearranged. The CP Hamiltonian is, therefore, the only one among all SSA Hamiltonians obeying the condition (4.13).

[22] S. F. Edwards, Proc. Roy. Soc. (London) **A267**, 518 (1962).
[23] N. F. Mott and H. Jones, *Theory of the Properties of Metals and Alloys* (Dover Publications, Inc., New York, 1958).

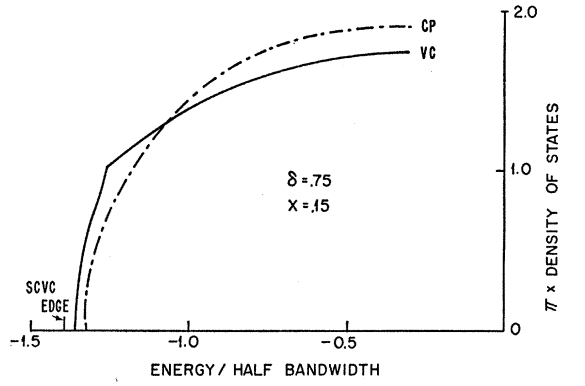

FIG. 2. Density of states near the lower band edge compared when coherent potential (CP) and virtual-crystal (VC) approximations are applied to a simple unperturbed density of states, with $\delta=0.75$, $x=0.15$. The location of the band edge in the self-consistent virtual crystal approximation (SCVC) is also indicated.

It is of interest to compare the limiting behavior corresponding to the dilute alloy, virtual crystal, and atomic limit obtained from Eq. (4.23) with the results given in (4.18)–(4.21). For the dilute alloy, $x\ll 1$, Eq. (4.23) becomes

$$\Sigma(z)=\epsilon+x\delta^2F^{(0)}(z-\Sigma)[1-\delta F^{(0)}(z-\Sigma)]^{-1} \quad (4.25)$$

to lowest order in x. Similarly in the virtual crystal, $\delta\ll 1$, and

$$\Sigma(z)=\epsilon+xy\delta^2F^{(0)}(z-\Sigma) \quad (4.26)$$

to second order in δ. Finally, in the atomic limit, $w\to 0$, $F^{(0)}(z)\sim z^{-1}$. Substitution in (4.23) leads to a result identical to (4.21). Equations (4.25) and (4.26) are seen to be self-consistent versions of (4.18) and (4.20) in the sense that ϵ^B and ϵ, respectively, in the arguments $F^{(0)}$, are replaced by Σ. An iterative solution of (4.25) and (4.26) yields (4.18) and (4.20) in lowest order. Therefore, the coherent potential approximation represents an interpolation scheme that reduces properly to the exact solutions in very diverse limiting cases. These correspond to the labelled boundaries of the $x-\delta$ plot in Fig. 1. It should be noted that we have no corresponding exact solution for the split-band limit. In fact the interpolation scheme is less suitable in the regime corresponding to $\delta\gg 1$ and w finite. We shall return to this point later.

When the coherent potential approximation is employed, the description is better than the non-self-consistent results for the limiting cases in question. This can be seen by comparing the approximate moments of the density of states μ_p with their exact counterparts derived in Sec. III B. The results are shown in Table I, which shows the number of lowest moments that are given correctly in various approximations. The details of the calculation are unimportant for the present purposes. Only the coherent potential case presents any difficulty and this will be discussed in Sec. IV D. In the first case the band is shifted rigidly and accordingly only its weight is correctly given. By contrast in the remaining cases the band is allowed to deform. This deformation becomes more precise as the approximation is refined and results in the fact that more moments are given correctly.

TABLE I. Number of exact moments of the total density of states in various approximations

Approximation	Number of exact moments
Rigid-band, Eq. (4.19)	2
Non-self-consistent virtual crystal, Eq. (4.20)	3
Self-consistent virtual crystal, Eq. (4.26)	3
Coherent potential, Eq. (4.23)	≥ 6

The self-consistency improves not only the general shape of the density of states which is reflected in the lowest moments, but also fine structural details. This is illustrated in Fig. 2 which compares $\rho(E)$ in the vicinity of the lower band edge for the last three cases listed in Table I. It is seen that in the non-self-consistent case there is parasitic structure in ρ at the rigid-band edge due to the fact that quasiparticles decay into bare particle states. By contrast in the self-consistent model both the band edge and the decay thresholds coincide because quasiparticles decay into other quasiparticle states.[24] The same is true for the self-consistent virtual-crystal model, only the edge is shifted slightly.

We now turn to a numerical comparison of three approximations, the self-consistent virtual crystal, the coherent potential, and the limit described by Eq. (4.21), which Soven[1] has called "the average t matrix" approximation.[4] A simple symmetrical single-band model, to be described explicitly in Sec. IV C is used here for illustrative purposes. The details of the model are unimportant in the present discussion since its only purpose is to characterize the general features of the three approximations. It should be emphasized that since the energy scale is such that $w=1$, the regime of large δ corresponds to the split-band limit.

The results for the density of states in the three cases are given in Figs. 3(a), 3(b), and 3(c), respectively. We shall describe the figure in two stages, comparing first the self-consistent virtual crystal (SCVC) and subsequently the average t-matrix approximation to the full self-consistent solution. Whereas the last exhibits the development, for increasing δ, of the band from the virtual crystal regime, through a stage where the single band is distorted at its upper edge, until it splits, the SCVC behavior is characterized by a band that is always symmetrical, never splits, but only broadens as δ increases. For large δ this approximation violates the localization theorem of Sec. III A.

The corresponding comparison of the averaged t matrix approximation is more interesting. Figure 3(c) shows that the bands always split. The reason for this

[24] The analogous situation in polaron theory has been discussed by G. Whitfield and R. D. Puff, Phys. Rev. **139**, A338 (1965).

can be inferred from Eq. (4.21), which shows that $\Sigma(z)$ always has a pole at $z=-\epsilon$ no matter how small δ becomes. Such a pole implies that ρ vanishes in its vicinity. By contrast in the CP case Sec. IV D will show that a pole in $\Sigma(z)$ appears only if δ is sufficiently large. The fact that the results of the averaged t-matrix approximation should be incorrect for small δ is not surprising in view of its breakdown. For intermediate values of δ, both approximations are qualitatively similar. However, a detailed comparison shows that the weights of the sub-bands are correctly given only in the CP approximation. As we approach the split-band limit, the weights of the sub-bands in the averaged t-matrix approximation become asymptotically correct, but the higher moments of the sub-bands remain incorrect. By contrast, the first and second moments in the CP approximation are exact. In particular, the shapes of the sub-bands satisfy the $\lambda_1=\lambda_2=\sqrt{x}$ relations of Eqs. (3.45) and (3.46). In the other approximation, $\lambda_1=1$ and $\lambda_2=x$, as was first inferred by Hubbard.[10] Of course even the CP approximation neglecting, as it does, molecular clustering, is not expected to be correct in the split-band limit. However, the preceding arguments should suffice to show that it is certainly better as an interpolation scheme than any other approximation presently available.

Because of the many advantages of the CP approximation given in this section, we shall present the discussion of the single-particle properties of our model alloy within its framework. The following three subsections will be devoted to these matters.

C. Model Density of States

In this subsection we introduce a specific model for which the numerical examples presented in the rest of the paper are computed. Equations (4.23) and (4.2) show that x, δ, and $\rho^{(0)}(E)$ completely determine $\Sigma(z)$. This permits us to start with a simple form for $\rho^{(0)}(E)$, rather than explicit $s(k)$, which would amount to complete specification of W. We assume for $\rho^{(0)}$ the form suggested by Hubbard[13]:

$$\begin{aligned}\rho^{(0)}(E)&=(2/\pi w^2)(w^2-E^2)^{1/2}, \quad |E|\leq w\\ \rho^{(0)}(E)&=0, \quad |E|>w\end{aligned} \tag{4.27}$$

which is symmetric,

$$\rho^{(0)}(E)=\rho^{(0)}(-E), \tag{4.28}$$

and has a simple shape against which all distortions due to alloying are clearly revealed. Because of (4.28), all symmetries discussed in Sec. III A apply, and we need only consider one quadrant of Fig. 1. In the numerical examples below, the parameters are restricted to $0\leq x\leq\frac{1}{2}$ and $0\leq\delta$. With these restrictions, the A atoms are impurities in a host B lattice and the most important effects associated with the impurities will appear at the top of the host band or above it.

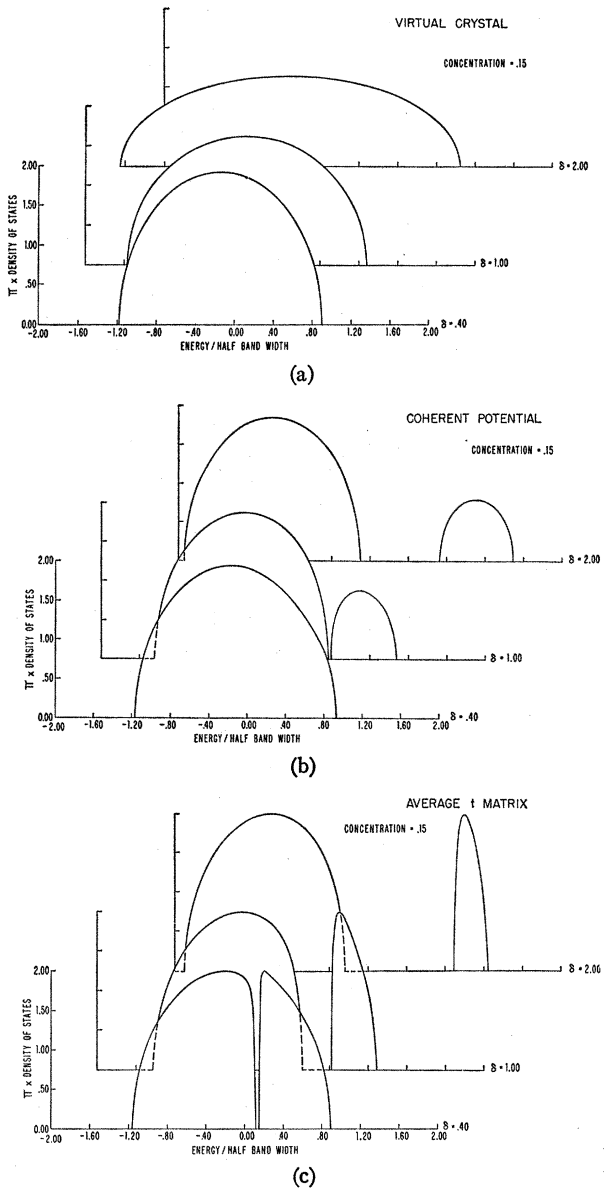

FIG. 3. Comparison of the density of states as calculated in (a) self-consistent virtual-crystal approximation, (b) coherent-potential approximation, and (c) average t-matrix approximation. In each case, $x=0.15$; the values of δ are 0.4, 1.0, and 2.0.

It should also be noted, as shown in Appendix D, that one can always find a dispersion law $s(k)$ which yields the model density of states $\rho^{(0)}(E)$ to arbitrary precision, despite the fact that $\rho^{(0)}$ has no critical points except at the band edges.

The function $F^{(0)}(z)$ yielding the form (4.27) for $\rho^{(0)}(E)$ [via (3.17)] is seen to be

$$F^{(0)}(z)=(2/w^2)[z-(z^2-w^2)^{1/2}]. \tag{4.29}$$

$F^{(0)}$ is analytic everywhere in a z-plane cut from $-w$ to $+w$, and vanishes as z^{-1} when $|z|\to\infty$. Substituting

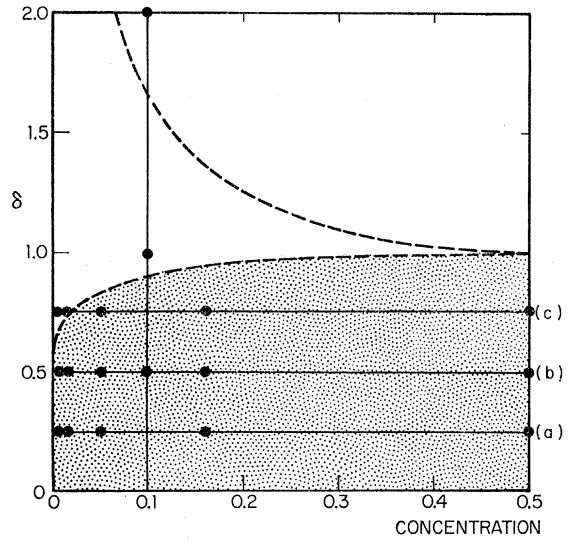

FIG. 4. Regimes of the coherent potential approximation for the model density of states (4.27). In the shaded region, the band is unsplit. Above the upper dashed line, a pole in the self-energy appears between the two sub-bands. The heavy dots indicate the values of x and δ at which the numerical results in Figs. 5–7 were obtained.

(4.29) into (4.23) yields a cubic equation for $\Sigma(z)$,

$$(z+\epsilon)\Sigma^3-[z\epsilon+\tfrac{1}{4}(\delta^2-1)]\Sigma^2+[\tfrac{1}{4}\delta^2(z+\epsilon)+\tfrac{1}{2}\epsilon]\Sigma +\tfrac{1}{4}[\delta^2(z\epsilon+\tfrac{1}{4}\delta^2)+\epsilon^2]=0, \quad (4.30)$$

expressed in units for which $w=1$. Alternately, we may invert (4.29) to obtain $\Sigma(z)$ as a function of $F^{(0)}[z-\Sigma(z)]$,

$$\Sigma(z)=z-[F(z)]^{-1}-\tfrac{1}{4}F(z), \quad (4.31)$$

and then substitute (4.31) into (4.23). The result is a cubic equation for $F(z)$,

$$\tfrac{1}{16}F^3-\tfrac{1}{2}zF^2+[z^2-\tfrac{1}{4}(\delta^2-1)]F-(z+\epsilon)=0. \quad (4.32)$$

Equations (4.30) and (4.32) may now be solved for real z, yielding for both either three real roots or one real root and a complex pair. When (4.30) or (4.32) has a complex pair of roots, the one in the lower half-plane is the physical one, since it will yield a non-negative density of states. When the roots are all real, the physical branch must be identified from its asymptotic behavior. The correct $F(z)$ will tend to zero, and the correct $\Sigma(z)$ to ϵ, as $z\to\pm\infty$. In a gap between split bands, continuity conditions isolate the correct root.

In practice, it is most convenient to solve Eq. (4.32) for $F(z)$, since $F(z)$ never has a pole. Equation (4.31) may then be used to obtain $\Sigma(z)$.

D. k-Independent Properties of the CP Approximation

This subsection and the next will consider the properties of the coherent-potential approximation. The general properties of our single-band model, all derived from (4.23), will be examined first, and then illustrated by numerical examples in which we specialize to the model density of states introduced in Sec. IV C. The simpler k-independent quantities, $\Sigma(z)$, $\rho(E)$, and $\rho^{A,B}(E)$, are discussed in this subsection; the k dependent properties, all developed from $\mathfrak{A}(k,z)$, are reserved for Sec. IV E.

By developing the asymptotic properties of the self-energy using Eq. (4.23), we may compare the results of the CP approximation with the exact results given in Sec. III B. Because $\Sigma(z)\to\epsilon$ as $|z|\to\pm\infty$, $|z-\Sigma(z)|\to\infty$, and $F(z)\equiv F^{(0)}(z-\Sigma)$ may be expanded in powers of $(z-\Sigma)^{-1}$ in that limit. This expansion may be written with the help of (3.24) and (3.27) in terms of the moments of the pure-crystal band in the form

$$F(z)=\textstyle\sum_{p=0}^{\infty}[z-\Sigma(z)]^{-p-1}\mu_p^{(0)}. \quad (4.33)$$

If we substitute (4.33) into (4.23), and expand $\Sigma(z)$ as

$$\Sigma(z)=\epsilon+\sigma_1 z^{-1}+\sigma_2 z^{-2}+\sigma_3 z^{-3}+\sigma_4 z^{-4}+O(z^{-5}), \quad (4.34)$$

the σ_p may be determined by matching coefficients of z^{-p} on both sides of Eq. (4.23). The resulting expansion of the self-energy,

$$\Sigma(z)=\epsilon+xy\delta^2[z^{-1}-\epsilon z^{-2}+(\epsilon^2+\mu_2^{(0)})z^{-3} +(\mu_3^{(0)}-\epsilon^3-\epsilon\mu_2^{(0)})z^{-4}]+\cdots, \quad (4.35)$$

is identical to order z^{-4} with the exact result (3.34). This procedure also yields the related entries of Table I.

The pole in $\Sigma(z)$ which appears near $z=-\epsilon$ in the split-band limit, as found in (3.52), is also present in the coherent potential approximation. To show this, we express $\Sigma(z)$ in the form

$$\Sigma(z)\approx A(z-a)^{-1} \quad (4.36)$$

appropriate near $z=a$ when the pole is present and located at a. Since $|z-\Sigma(z)|\to\infty$ near the pole, we may use expansion (4.33) for $F^{(0)}[z-\Sigma(z)]$ near $z=a$. Substitution of Eq. (4.36) and the first three terms of Eq. (4.33) into Eq. (4.23) determines A and a. We find

$$\Sigma(z)\approx(xy\delta^2-\mu_2^{(0)})(z+\epsilon)^{-1}, \quad (4.37)$$

which is identical with the result, exact to order δ^{-2}, already given as (3.55). In the CP approximation, therefore, the pole appears at $z=-\epsilon$, if at all, and does not shift with x or δ. The requirement that $\mathrm{Im}\Sigma(E+i0)\leq 0$ provides a (necessary) condition

$$xy\delta^2\geq\mu_2^{(0)} \quad (4.38)$$

for the existence of the pole.

For numerical examples, we now specialize to the model $F^{(0)}$ given in (4.29) and present the results of solving (4.30) and (4.32) for $\Sigma(z)$ and $F(z)$. The values of x and δ for which we exhibit calculations are indicated by heavy dots in Fig. 4, which is just the upper left quadrant of Fig. 1, enlarged.

Figures 5(a)–5(c) show the self-energy $\Sigma(z)$ calculated for $x=0.1$ and three values of δ. These cases, on the vertical line in Fig. 4, exhibit all the varieties of be-

havior to be found in $\Sigma(z)$ for general x and δ. Figure 4 is divided by dashed lines into three regions, each typified by one of the Figs. 5. In the lowest, shaded region, $\Sigma(z)$ has a single cut along the real axis, and an unsplit band results.[25] In the middle region there are two cuts (a split band), while in the top region a pole separates the two cuts. One can show from (4.32) that, for this choice of $F^{(0)}(z)$, the condition (4.38) is also sufficient for the appearance of the pole in $\Sigma(z)$. Since $\mu_2^{(0)}=\frac{1}{4}$ for the model density of states (4.27), the upper dotted line in Fig. 4 is given by $xy\delta^2=\frac{1}{4}$.

The simplest case is Fig. (5a), in which $\delta=0.5$ and the band is not split. In the lower part of the band ImΣ is relatively small and ReΣ nearly constant, although not quite equal to $\epsilon=0.2$. This behavior is characteristic of the virtual crystal limit. At the higher energies, the impurities produce a rapidly varying ReΣ and large values of ImΣ. The increase in ImΣ, indicating that states near the top of the band are preferentially damped by the impurities, is observed for the smallest values of δ studied. Increasing δ to 1.02, in Fig. 5(b), splits off a sub-band, and the strongest damping occurs near the gap edge of that impurity sub-band. The majority sub-band for the most part displays the "virtual-crystal" behavior already noted in Fig. 5(a). For the largest δ considered, namely, $\delta=2.0$ in Fig. 5(c), $\Sigma(c)$ has a pole at $-\epsilon=0.8$. Although the lower sub-band in Fig. 5(c) is not very different from that of Fig. 5(b), ImΣ in the impurity sub-band has increased by a factor of roughly 4.

The relation between Figs. 5(b) and 5(c) may be understood in terms of the sum rules involving ImΣ. When $\rho^{(0)}$ is given by (4.27), the sum rule (3.58) for the lower sub-band, which is exactly valid only for large splittings, is nevertheless satisfied in the CP approximation as soon as the impurity sub-band has split off. Thus ImΣ in the majority sub-band cannot differ markedly in the two cases. Because the appearance of the pole causes the integral of ImΣ over the two bands to saturate at the value $-\pi\mu_2^{(0)}$ which is independent of δ [cf. (3.56)], ImΣ in the impurity sub-band increases rapidly with δ only in the middle region of Fig. 4. For the $\delta=2.0$ characterizing Fig. 5(c), this saturation has occurred, and the sum rule (3.58a) for the α sub-band is satisfied as well.

We now turn to a discussion of the total and component densities of states, $\rho(E)$, $\rho^A(E)$, and $\rho^B(E)$, as defined by (3.17) and (4.15). These quantities are plotted[26] as Figs. 6 and 7, respectively, for three values of δ, all less than 1. For each δ, results for a set of concentrations are given, with values of x spaced logarithmically to emphasize the transition from the dilute to the nondilute alloy region.

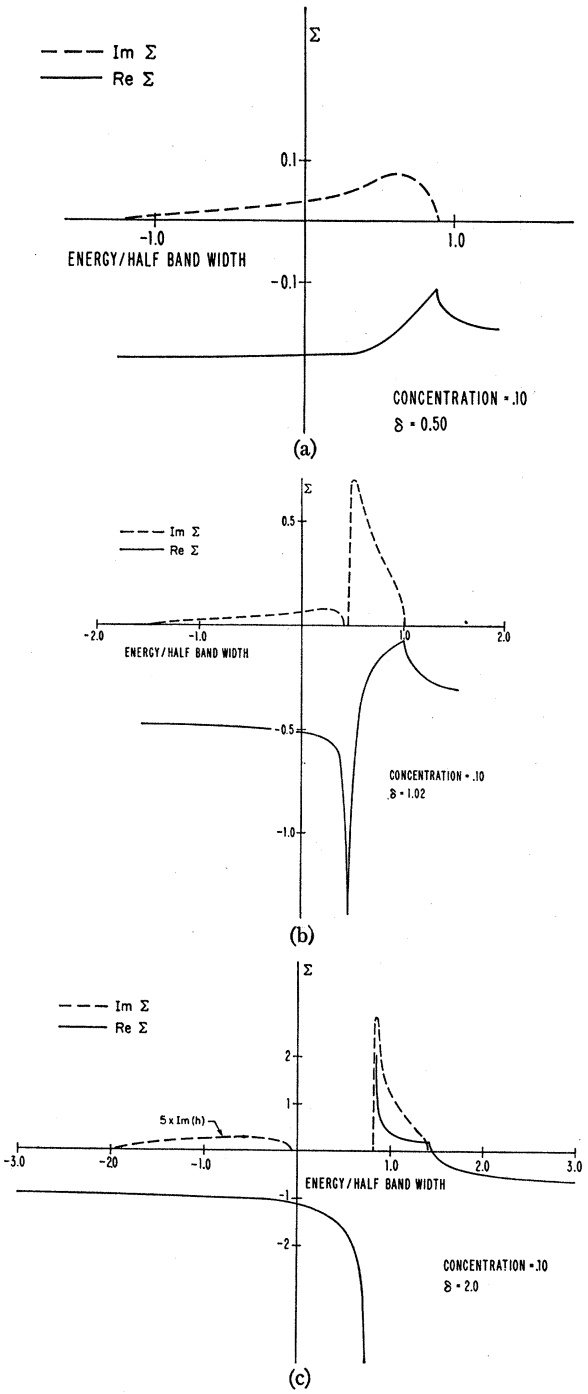

FIG. 5. The real (solid line) and the absolute value of the imaginary (dashed line) parts of the self-energy in the coherent-potential approximation calculated for $x=0.1$ and (a) $\delta=0.5$, (b) $\delta=1.02$, (c) $\delta=2.0$. These correspond to points on the vertical line in Fig. 4 and typify the three regimes. Note the changes of scale in these three figures.

The restriction to small δ was motivated by the fact that the SSA is likely to be best when the two types of atoms present do not differ too greatly. Under these circumstances, the fluctuations due to the nearby en-

[25] This region was previously identified in Ref. 9.

[26] The "three-dimensional" graphs of Figs. 3, 6, and 7 are tracings of machine output prepared with remarkably little effort or expense on an IBM 7094 computer with Calcomp plotting accessories.

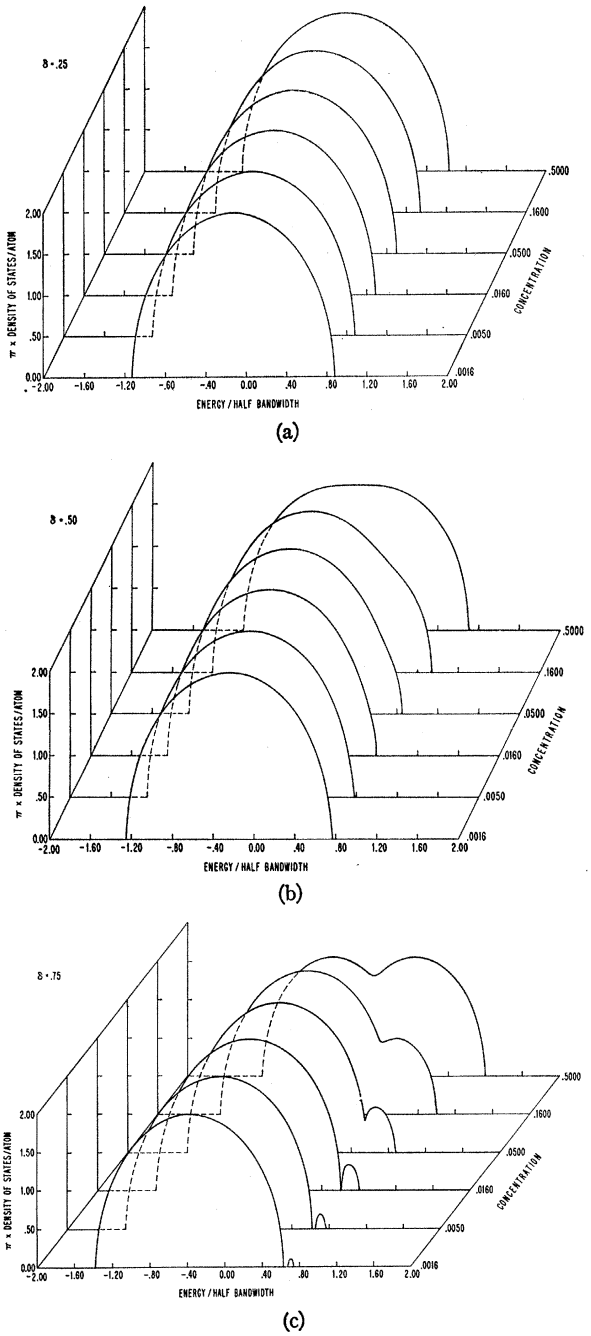

FIG. 6. Density of states calculated with the model $\rho^{(0)}(E)$ given by (4.27) in the coherent-potential approximation, for a variety of concentrations along the lines (a), (b), and (c) of constant δ in Fig. 4; (a) $\delta=0.25$, (b) $\delta=0.5$, and (c) $\delta=0.75$.

vironment, neglected in (2.19) to yield (2.20) and (2.23), are most likely to be small. We show results for various values of the parameter x because this corresponds to the experimental possibility of making samples with different concentration ratios.

Figure 6(a) corresponds to $\delta=0.25$ and reflects behavior characteristic of the virtual crystal limit. The parameters used in these graphs are shown by dots on the bottom horizontal line in Fig. 4. The only visible effects of alloying are a concentration-dependent broadening and shift of the band center of gravity given by $\epsilon=(x-y)\delta/2$. In Fig. 6(b), $\delta=0.5$, and some distortion of the band shape is evident. This distortion is localized near the upper edge for small x and spreads over larger portions of the band with increasing concentration. It is most evident in the curves for $x=0.05$ and 0.16.

When δ is increased to 0.75, then, as shown in Fig. 4, an impurity band splits off the upper edge of the host band. This is the situation considered in Fig. 6(c). The width and height of the impurity sub-band are proportional to $\sqrt{x}$ for small x, and remain approximately so until the bands merge. The integrated density in the impurity sub-band is x within numerical accuracy in the split-band region.

The results of these calculations differ from those of the rigid-band model for alloys. This model has been questioned on grounds that effects associated with changes in the average crystal potential and broadening due to fluctuations should alter the shape of the band in the alloy.[27,28] In addition, the rigid-band model assumes that all sites are equivalent, as in a perfect crystal. Its limited empirical successes[29] do not imply uniqueness. In fact, a "minimum polarity" model which destroys site equivalence by insisting on local charge neutrality has proven successful in predicting several electronic properties of NiCu alloys.[27]

The first objection to the rigid-band model, that $\rho(E)$ is distorted, is clearly sustained by Figs. 6(a)–6(c). To explore the inequivalence of the A and B sites, we must calculate the component densities of states, $\rho^A(E)$ and $\rho^B(E)$, given for the CP model by (4.15). These are plotted in Figs. 7(a)–7(c), for the same values of δ and x as in Figs. 6(a)–6(c). The total density of states is obtained from ρ^A and ρ^B by

$$\rho(E)=x\rho^A(E)+y\rho^B(E). \tag{4.13}$$

Only ρ^A, represented by solid lines in Fig. 7, contains any sharp structure. By contrast, the behavior of ρ^B arising from the host atoms is much more like that in a virtual crystal, particularly for small x. Accordingly, the structure seen in the corresponding ρ is due to the A sites. Even in the virtual crystal limit, Fig. 7(a), ρ^A is distorted, peaking at the higher energies. This behavior contradicts the rigid-band assumption that sites are equivalent.

The quantities ρ^A and ρ^B also provide insight into the dilute alloy limit. Within the coherent potential approximation it is true in general, according to (4.23), that as $x\to 0$, $\Sigma(z)\to\epsilon$. Thus (4.15) leads to the limiting

[27] N. D. Lang and H. Ehreneich, Phys. Rev. **168**, 605 (1968).
[28] D. H. Seib and W. E. Spicer, Phys. Rev. Letters **20**, 1441 (1968).
[29] J. Friedel, Nuovo Cimento Suppl. **7**, 287 (1958).

forms

$$\rho^B(E) = -\pi^{-1}\,\mathrm{Im}F^{(0)}(E-\epsilon^B+i0) = \rho^{(0)}(E-\epsilon^B)\,,$$
$$\rho^A(E) = -\pi^{-1}\,\mathrm{Im}\{F^{(0)}(E-\epsilon^B+i0) \times[1-\delta F^{(0)}(E-\epsilon^B+i0)]^{-1}\}\,. \quad (4.39)$$

The expression for ρ^A is seen to be just the Koster-Slater formula[15] for the density of states at a single impurity, whereas ρ^B has become the unperturbed B crystal density of states. Figures 7(a) and 7(b) demonstrate these low concentration limits. It can be seen in Fig. 7(c), however, that the impurity band remains broader than the δ function predicted by the one-impurity Koster-Slater model. This is a general result for any effective wave theory, since the effective medium broadens an impurity level at any concentration. Because of the possibility of electron hopping between sites, some broadening of the impurity level would be expected at any finite concentration. However, the CP approximation overestimates this broadening by using effective atoms, each of which possesses some impurity character and facilitates hopping over short distances.

E. k-Dependent Properties of the CP Approximation

The preceding subsections have compared the CP approximation with other single site approximations and discussed its consequences for the k-independent quantities, as, for example, the densities of states per atom. This subsection will be devoted to a discussion of the entire averaged Green's function

$$\mathcal{G}(k,z) = [z - s(k) - \Sigma(z)]^{-1} \quad (3.9)$$

as calculated for the model density of states (4.27) in the CP approximation. $\mathcal{G}(k,z)$ contains full information about the one-particle properties of this model, and in particular permits discussion of the quasiparticle approximation. In virtue of the properties of $\langle G\rangle$, the quasiparticle states are Bloch waves $|k\rangle$. Because $\Sigma(z)$ is k-independent in the coherent potential approximation, $\mathcal{G}(k,z)$ depends upon k only through $s(k)$, which ranges from -1 to $+1$.

We begin by plotting two numerical examples of $\mathcal{A}(k,z)$ defined in (3.10). By (3.11), $\mathcal{A}(k,z)$ completely determines $\mathcal{G}(k,z)$. In the first example, shown in Fig. 8(a), where $x=0.05$ and $\delta=2.0$, x has been chosen fairly small, and δ large enough to guarantee that the impurity sub-band has split off. We expect that in the spectral density two kinds of excitation will appear, one related to the plane-wave-like eigenstates of the pure B crystal, the other to the impurity states. In Fig. 8(a) this occurs: For each k, represented by the corresponding $s(k)$, there are two peaks in $\mathcal{A}(k,z)$. The lower peak has a quasiparticle character, being well localized in k space as well as in energy, and having a generally Lorentzian shape except at the band edge. Its center moves to higher energies as $s(k)$ increases. By contrast, the upper peak of $\mathcal{A}$ does not shift with $s(k)$ and the

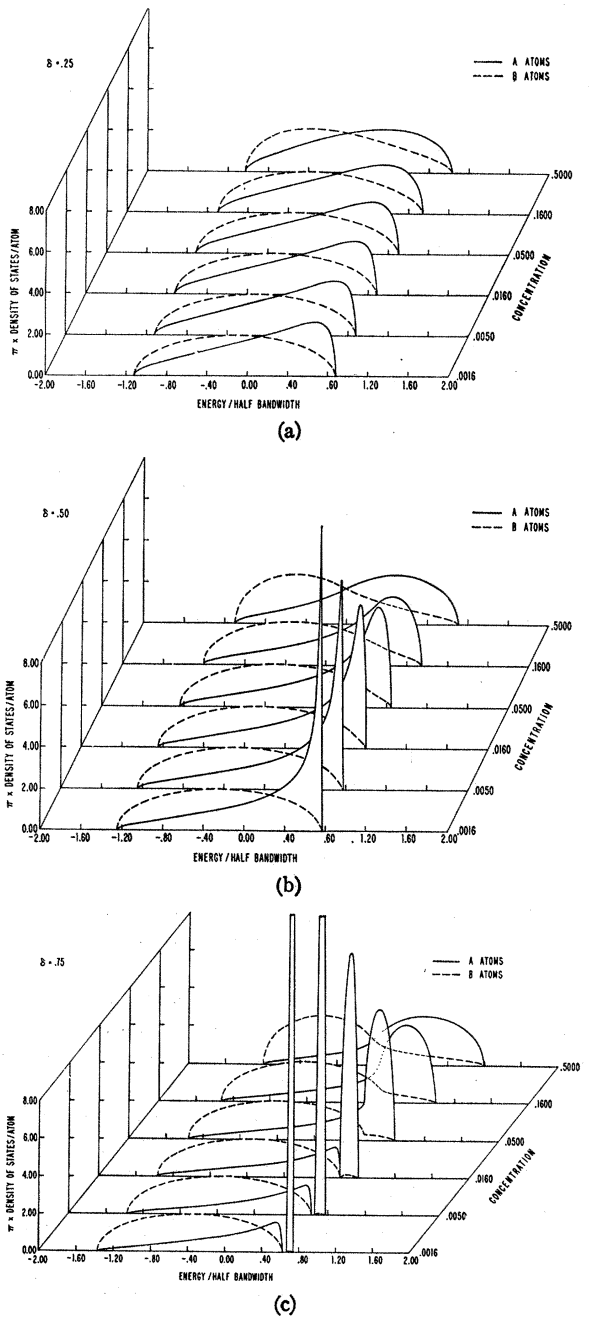

FIG. 7. Component densities of states, ρ^A (solid lines) from the minority sites, and ρ^B(dashed lines) from the majority sites, as defined in (4.15). Values of x and δ are the same as in Figs. 6(a)–6(c).

shape of $\mathcal{A}$ is quite different. The flatness of the upper sub-band in k space and its extent over the entire band is that expected of states localized in coordinate space. The strongly damped, non-Lorentzian character of the states is consistent with the behavior of $\Sigma(z)$ shown in Figs. 5(b) and 5(c).

It is interesting that this behavior in $\mathcal{A}$ is also exhibited when δ is decreased to 0.75, $x=0.15$ [in Fig.

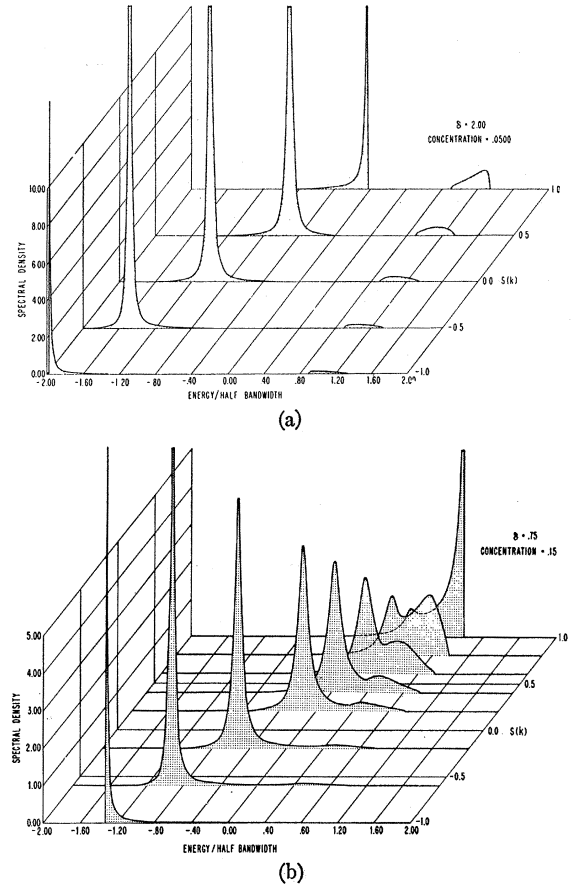

FIG. 8. Spectral density $\mathcal{A}(k,E)$ versus E at several values of $s(k)$ for (a) $\delta=2.0$, $x=0.05$, and (b) $\delta=0.75$, $x=0.15$.

8(b)], and the impurity band is no longer split off. As before, quasiparticle behavior is evident near the bottom of the band, but this is disturbed very strongly in the vicinity of $s(k)=+1$. In contrast to Fig. 8(a), however, the influence of the impurity extends only over a smaller portion of k space. This greater localization in k space of the states associated with ϵ^A implies a greater degree of delocalization of the states in coordinate space. This behavior of course is just that to be expected as ϵ^A and ϵ^B move energetically closer and the concentration of B sites increases, thereby making hopping between them easier.

We should expect the qualitative quasiparticle behavior discussed above to coincide with the appearance of poles in the continuation of $\mathcal{G}(k,z)$ into the lower half z plane. Such poles will be located at z given by

$$z-\Sigma(z)=s(k). \tag{4.40}$$

To determine z, (4.40) may be substituted into the continuation of (4.23). The resulting quadratic equation for z is easily solved. For $xy\delta^2$ small, the physical root is given by

$$z_1(k)\approx\epsilon+s(k)+xy\delta^2F^{(0)}[s(k)+i0]. \tag{4.41}$$

As $xy\delta^2\to 0$, this root tends to the virtual crystal eigenvalue $\epsilon+s(k)$. Thus we may interpret $z_1(k)$ as a quasiparticle energy. The other root has no clear relationship to the structure of $\mathcal{A}(k,E)$. In particular the impurity region of the spectrum is not associated with a pole. This is an expected result, since the impurity region of $\mathcal{A}(k,E)$ shown in Fig. 8 was non-Lorentzian.

Unfortunately, when $xy\delta^2$ is not small, neither pole may have a clear interpretation. This could represent a breakdown of the quasiparticle concept for strong coupling. More likely, it is the nature of the coherent potential approximation which limits the identification. We have not been able to resolve this ambiguity.

The difficulties of interpreting the most detailed single-particle properties that result from the CP approximation represent no bar to the calculation of grosser physical quantities which bear more directly on observable properties of the system. One important example is the distribution function of Bloch states in the bands, which proves to be rather insensitive to the fine details of $\mathcal{A}(k,E)$. At 0°K, the Fermi energy is determined by the equilibrium electron concentration per atom and per spin, c, according to

$$c=\int_{-\infty}^{E_F}\rho(E)dE. \tag{4.42}$$

The average occupation number for each Bloch state is

$$\langle n_k\rangle=\int_{-\infty}^{E_F}dE\mathcal{A}(k,E). \tag{4.43}$$

As before, $\langle n_k\rangle$ depends on k only through $s(k)$, and therefore is constant in k space on surfaces of constant $s(k)$. Accordingly, it sufficies to consider $\langle n_k\rangle$ as a function of $s(k)$. Figure 9 shows such a plot for various values of E_F, and the same δ and x as in Fig. 8(b). In contrast to the behavior characterizing the k dependence of the Fermi distribution at 0°K in the pure crystal, quasiparticle broadening effects prevent the $\langle n_k\rangle$ of Fig. 8(b)

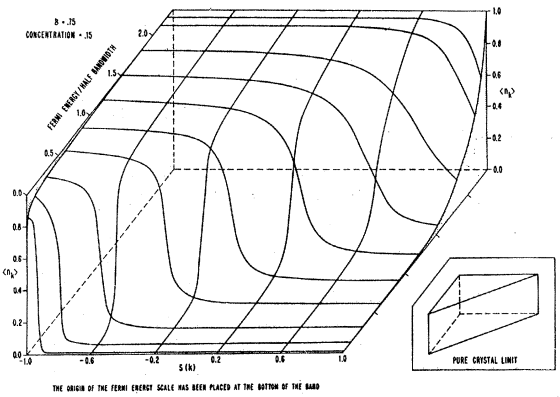

FIG. 9. Distribution function $\langle n_k\rangle$ at $T=0$°K versus $s(k)$ (horizontal axis) and E_F (slanted axis), for $\delta=0.75$, $x=0.15$ as in Fig. 8(b). The origin of the E_F scale is at the bottom of the band.

from falling off abruptly. As an aid in visualizing the degree of broadening, the results corresponding to the pure-crystal limit have been sketched in the inset. In this limit

$$\begin{aligned}\langle n_k\rangle&=1, \quad s(k)\leq E_F\\ \langle n_k\rangle&=0, \quad s(k)>E_F.\end{aligned} \tag{4.44}$$

The localized impurity state clearly visible in Fig. 8(b) near the top of the band produces only extra broadening of the distribution function near the top of the band. The width of $\langle n_k\rangle$ obtained in Fig. 9 increases from about 5% of the bandwidth near the lower-band edge, where the peaks in $\mathcal{A}(k,E)$ are quite narrow, to about 30% near the upper edge.

APPENDIX A: PROPERTIES AND EXAMPLES OF SYMMETRIC BANDS

We define symmetric bands as those for which a vector κ exists such that

$$s(k)=-s(k+\kappa), \quad \text{for all } k. \tag{A1}$$

A direct consequence of (A1) is that the crystal density of states is symmetric,

$$\rho^{(0)}(E)=\rho^{(0)}(-E). \tag{A2}$$

The symmetry of $\mathcal{G}$ implied by (A1) is

$$\mathcal{G}(k,z|x,\delta)=-\mathcal{G}^*(k-\kappa,-z^*|x,-\delta). \tag{A3}$$

From this equation together with (3.19), Eqs. (3.20) and (3.21) are obtained.

From (A1), it follows $s(k+2\kappa)=s(k)$ so that κ is half of a reciprocal-lattice vector. Although symmetric bands are rare in nature, they appear in the simplest cases of nearest-neighbor tight-binding approximation.

For example, in the simple cubic lattice,[23]

$$s(k)=\tfrac{1}{3}(\cos k_x a+\cos k_y a+\cos k_z a)$$

and $\kappa=(\pi/a)(1,1,1)$. In the bcc lattice,

$$s(k)=\cos\tfrac{1}{2}k_x a\,\cos\tfrac{1}{2}k_y a\,\cos\tfrac{1}{2}k_z a$$

and $\kappa=(2\pi/a)(1,0,0)$.

APPENDIX B: COMPUTATION OF $\langle H^p\rangle$

Using (3.2), we write

$$\langle H^p\rangle=\langle(D+W)^p\rangle=\langle D^p\rangle+\langle DW^{p-1}\rangle+\cdots+\langle W^p\rangle. \tag{B1}$$

Each of the 2^p averages is performed separately. This can be done for small p. The following examples, relating to $p=4$, illustrate the procedure used. Properties of D and W described in Sec. III A, in particular, (3.1) and (3.6), are employed as well as definitions (3.27), (3.28), and the useful identity

$$\tfrac{1}{4}\delta^2=\epsilon^2+xy\delta^2. \tag{B2}$$

The Wannier representation is used:

$$\begin{aligned}(\langle D^4\rangle)_{nm}&=\langle\epsilon_n{}^4\rangle\delta_{nm}=([\tfrac{1}{2}\delta]^4\mathbf{1})_{nm},\\ (\langle D^3W\rangle)_{nm}&=\langle\epsilon_n{}^3\rangle t_{nm}=(\epsilon[\tfrac{1}{2}\delta]^2W)_{nm},\\ (\langle DWDW\rangle)_{nm}&=\textstyle\sum_{q\neq m}\langle\epsilon_n\epsilon_q\rangle t_{nq}t_{qm}\\ &=(\epsilon^2W^2)_{nm},\\ (\langle DW^2D\rangle)_{nm}&=\langle\epsilon_n\delta_m\rangle(W^2)_{nm}\\ &=(\epsilon^2W^2+xy\delta^2\mu_2{}^{(0)}\mathbf{1})_{nm}.\end{aligned}$$

Averages appearing in (A4) for any p less than 7 may be determined in the indicated way. For higher p correlation of several sites becomes important and the results are not obtained in the simple way shown above.

APPENDIX C: IDENTIFICATION OF EQ. (4.24) WITH HUBBARD'S THEORY

The third of Hubbard's papers on electron correlation in narrow bands deals with the so-called alloy analogy: If one regards the down-spin electrons as fixed to randomly distributed sites, the motion of the up-spin electrons is identical to the motion of electrons in a model alloy system equivalent to that treated in the present paper. Part 4 of Ref. 13 deals with the "scattering correction," i.e., with the related alloy problem. Hubbard's approximate solution is given in Eqs. (37)–(40). Here, the dictionary is given which translates Hubbard's notation into that used in our paper.

$$\begin{aligned}&G_{\mathbf{k}}{}^{\sigma}(E)\rightarrow(2\pi)^{-1}\mathcal{G}(k,z), && \epsilon_{\mathbf{k}}-T_0\rightarrow s(k),\\ &G_{ii}{}^{\sigma}(E)\rightarrow F(z), && n_{-\sigma}{}^{+}\rightarrow x,\ \epsilon_{+}\rightarrow\epsilon^A,\\ &F_s{}^{\sigma}(E)\rightarrow z-\Sigma(z), && n_{-\sigma}{}^{-}\rightarrow y,\ \epsilon_{-}\rightarrow\epsilon^B,\\ & && I\rightarrow\delta.\end{aligned}$$

With these identifications, it is straightforward to show that Hubbard's Eq. (38) is identical to our Eq. (4.24).

APPENDIX D: CONSTRUCTION OF A BAND CORRESPONDING TO A GIVEN $\rho^{(0)}$

The dispersion law $s^{(0)}(k)$ corresponding to a given $\rho^{(0)}$ is not determined uniquely. The function $s^{(0)}(k)$ should be analytic and periodic in k space. We try to obtain $s^{(0)}(k)$ by deforming an arbitrarily chosen single band appropriate to a given crystal structure. Its dispersion law and density of states are denoted by $s(k)$ and $\rho(E)$ respectively. The correspondence of $s^{(0)}$ and s is assumed to have the form

$$s^{(0)}(k)=\varphi[s(k)]. \tag{D1}$$

The isoenergetic surfaces in k space are not deformed by (D1): The two surfaces

$$\begin{aligned}s(k)&=\eta=\text{const},\\ s^{(0)}(k)&=\varphi(\eta)=\text{const}\end{aligned} \tag{D2}$$

coincide. Therefore,

$$\nu(\eta)=\int_{-\infty}^{\eta} dE\rho(E)=\int_{-\infty}^{\varphi(\eta)} dE\rho^{(0)}(E). \qquad \text{(D3)}$$

This is an equation for φ. The function $\nu(\eta)$, the integrated density of states, increases smoothly from 0 to 1. If $\rho^{(0)}(E)$ is continuous, (D3) determines a unique smooth monotonic function φ. The $s^{(0)}(k)$ given by(D1) is then periodic in k space and smooth although in general not analytic: The second and higher derivatives may be discontinuous at critical points of both ρ and $\rho^{(0)}$. In practice, however, it is possible to fit $s^{(0)}(k)$ by an analytic function.

PHYSICAL REVIEW VOLUME 175, NUMBER 3 15 NOVEMBER 1968

Second- and Third-Order Elastic Constants of Alkali Metals*

TETSURO SUZUKI, A. V. GRANATO, AND J. F. THOMAS, JR.†
Department of Physics and Materials Research Laboratory, University of Illinois, Urbana, Illinois 61801
(Received 9 May 1968)

The second- and third-order elastic constants of lithium, sodium, potassium, and rubidium in the body-centered cubic structure are calculated. The relationship between Brugger elastic constants and Fuchs elastic constants is worked out. The Brugger elastic constants, which are defined as the derivatives of the energy with respect to the Lagrangian strain, are widely used to express experimental results. The Fuchs elastic constants, which are defined as the derivatives of the energy with respect to homogeneous expansion and volume-conserving homogeneous shear, are often more convenient for calculations in terms of atomistic considerations, and are particularly convenient for calculations with pseudopotentials. They are used here to calculate the contribution of the band-structure energy to the elastic constants using the local pseudopotential proposed by Ashcroft. This pseudopotential contains the core radius as the only adjustable parameter. The contribution of the band-structure energy to the elastic constants is represented as a summation of two kinds of derivatives of the wave-number characteristics over the reciprocal lattice points—those with respect to homogeneous expansion and those with respect to volume-conserving homogeneous shear. The core radius which gives the best fit to the experimental second-order elastic constants agrees with that determined by Ashcroft from data on the Fermi surface or on the resistivity of liquid metals. The band-structure energy term is found to make a small contribution to the second-order elastic constants but an indispensable contribution to the third-order elastic constants.

I. INTRODUCTION

THERE are two methods for calculating the second-order elastic constants of a crystal: the method of homogeneous deformation and the method of long waves. One should be able to calculate the second-order elastic constants using either of the two methods[1] and the results obtained should agree with each other if the same model of the crystal is used in both cases. Fuchs[2,3] calculated the second-order elastic constants of alkali metals by the method of homogeneous deformation and obtained a satisfactory comparison with the data available at that time. However, more recent calculations[4–7] of the second-order elastic constants of alkali metals have been mostly carried out by the method of long waves, except for the calculation of bulk moduli by Ashcroft and Langreth.[8]

Ho and Ruoff[6] based their calculation on a quite different model of an alkali metal which includes closed-core interactions instead of the free-electron energy. Therefore, their results cannot be directly compared with the present calculation. Shyu and Gaspari[5] calculated the effective interatomic potential for alkali metals from the Heine-Abarenkov model potential. They also calculated the second-order elastic constants from the effective interatomic potential by the method of long waves. Their results of the second-order elastic constants are not in as good agreement with the experimental data as the present results, although they used a more sophisticated pseudopotential than that used in the present calculation. However, this is not necessarily evidence against the Heine-Abarenkov pseudopotential,

* Supported by the U. S. Atomic Energy Commission under Contract No. AT(11-1)-1198.
† Present address: Department of Physics, University of Virginia, Charlottesville, Va.
[1] D. C. Wallace, Rev. Mod. Phys. **37**, 57 (1965).
[2] K. Fuchs, Proc. Roy. Soc. (London) **A153**, 622 (1936).
[3] K. Fuchs, Proc. Roy. Soc. (London) **A157**, 444 (1936).
[4] W. A. Harrison, *Pseudopotentials in the Theory of Metals* (W. A. Benjamin, Inc., New York, 1966), p. 195.
[5] W. Shyu and G. D. Gaspari, Phys. Rev. **163**, 667 (1967).
[6] P. S. Ho and A. L. Ruoff, Phys. Status Solidi **23**, 489 (1967).
[7] Besides the works which calculate the second-order elastic constants explicitly, there are many papers on the phonon-dispersion relationship which contain the second-order elastic constants implicitly. As sources for reference to these works we mention the following recent articles: R. A. Cowley, A. D. B. Woods, and G. Dolling, Phys. Rev. **150**, 487 (1966); in *Phonons in Perfect Lattice and in Lattices with Point Imperfections*, edited by R. W. H. Stevenson (Plenum Press, Inc., New York, 1966); in *Lattice Dynamics*, edited by R. F. Wallis (Pergamon Press, Inc., London, 1965).
[8] N. W. Ashcroft and D. C. Langreth, Phys. Rev. **155**, 682 (1967).